

Friedrich-Alexander University Erlangen-Nuremberg
Institute of Fluid Mechanics

Prof. Dr. Dr. h.c. F. Durst

**Evaluation of Improved Boundary Conditions
for the Lattice Boltzmann Approach:
Investigation of the Laminar Vortex Street
behind a Circular Cylinder**

**Bachelor's Thesis
Milena Gergova**

December 2002

Supervisors: Dipl.-Ing. Thomas Zeiser
Dr.-Ing. Gunther Brenner
Prof. Dr. Dr. h.c. Franz Durst

Contents

1	Introduction	1
1.1	Motivation	1
1.2	Aim of This Thesis	1
1.3	Outline	3
2	Vortex Shedding behind a Circular Cylinder	4
2.1	The Relevant Dimensionless Numbers	4
2.2	Flow Regimes Behind a Circular Cylinder	6
2.3	Influence of the Computational Domain on the Flow	9
2.4	Influence of Confining Walls	9
2.5	The Numerical Simulation of Vortex Streets — a Historic Overview	10
3	Introduction to the Lattice Boltzmann Approach	12
3.1	The Development of Lattice Gas Automata	12
3.2	The Background of the Microscopic Model of Fluids	13
3.3	The Lattice Gas Algorithm	14
3.4	The Lattice Boltzmann Approach	15
3.4.1	From Lattice Gas to Lattice Boltzmann	16
3.4.2	Discretization of the Boltzmann Equation	16
3.4.3	BGK Relaxation	17
3.4.4	Numerical Application of the Lattice Boltzmann Approach	17
4	Evaluation of the Vortex Shedding in a Channel	19
4.1	Investigated Reynolds Numbers	19
4.2	Schematic Presentation of the Channel	20
4.3	Boundary and Initial Conditions	20
4.4	Evaluation of the Detachment Frequency	21
4.5	Boundary Fitting Versus Bounce Back Boundary Conditions	25
5	Results and Discussions	29
5.1	Comparison of the Program Codes	29
5.2	Influence of the Domain Length	31

5.3	Influence of the Obstacle Size	33
5.4	Influence of the Blockage Ratio	34
5.5	Simulations at Reynolds = 131.9	36
5.6	Former Investigation of Circular Cylinder	36
5.6.1	Yokoi's Experimental Work	37
5.6.2	The Investigations of Williamson	37
5.6.3	Karniadakis and Triantafyllou's Numerical Study	38
5.6.4	The Numerical Research of Thompson et al.	38
5.6.5	Persillon and Braza's Numerical Simulation	39
5.6.6	Zovatto and Pedrizzetti's Study of Cylinder Between Parallel Walls	39
5.6.7	Juxtaposition of the Results	40
6	Summary	44
	Appendix	46
	Index of Figures	47
	Index of Tables	48
	Index of Symbols	49
	Greek Letters	50
	Dimensionless Numbers	50
	References	51

1 Introduction

1.1 Motivation

The study of viscous flow phenomena behind a circular cylinder has a long history dating back to the 19th century. Despite the geometrical simplicity, complicated flow phenomena occur which are related to the detachment of the flow and the time dependent vortex shedding. This simple geometrical setup is also the starting point for many more complex configurations including the flow in heat exchangers and vortex flow meters or around chimneys and towers. Therefore, this flow has motivated numerous scientists and engineers to investigate its physics and technical applications through theoretical, experimental and more recently, computational approaches.

The first milestone in this field was put by von Karman in 1912, who analyzed the stability of vortex street configurations and established a theoretical link between the vortex street structure and the drag on the body. Later in 1954 Roshko carried out extensive measurements of the vortex shedding. Over the last 50 years a great number of scientists like Williamson, Karniadakis and Triantafyllou, Coutanceau and Bouard, Fornberg, Chen and others were involved in the investigation of this flow, so nowadays a large number of works are available. Yet, most of them concentrate on an infinite flow domain. Confining walls however can have a big impact on the flow which results amongst other things in a parabolic inflow profile and an additional damping of disturbances in the flow field.

The flow in a confined domain is of interest for many technical applications, e.g. tubes of heat exchangers in cross flow. For computational fluid dynamics (CFD) investigations the well defined solid boundary in span-wise direction is also advantageous. Nowadays, many numerical approaches are available and applied to flow simulations. Especially during the last several years, discrete mesoscopic CFD methods, including the lattice gas automata (LGA), and the lattice Boltzmann approach (LBA), have attracted increasing attention. These lattice methods are based on a discrete particle description of the fluid. They provide many of the advantages of molecular dynamics such as clear physical pictures and are much easier to implement from the computational point of view. The resulting algorithms allow a fast and efficient simulations on modern computers. But as these methods are relatively new, there are still many open questions and possibilities for improvements. Especially the efficient handling of boundary conditions can be crafty.

1.2 Aim of This Thesis

The subject of this thesis is the investigation of the viscous flow around a circular cylinder in a channel at moderate Reynolds numbers using the lattice Boltzmann method. The Reynolds number range is chosen in such a way that the flow is time dependent, i.e. vortex shedding occurs. Thus, the lower limit is given by the critical Reynolds number Re_c . The upper limit for the Reynolds number is due to the fact that only two dimensional

calculations are carried out. Therefore, it is no use to go beyond a Reynolds number of about $Re_\infty = 150$ because above it, three dimensional flow phenomena, which cannot be recovered correctly by the two dimensional simulations, already begin to occur, long before the flow becomes turbulent at much higher Reynolds numbers.

The fluid mechanical aspect of this work is to investigate the influence of the channel walls and the blockage ratio (i.e. the ratio between the cylinder diameter and the channel height) on the critical Reynolds number and frequency of the vortex shedding. Only little information on this topic can be found in literature as most of the reported investigations focus on unbounded flows.

From the numerical point of view, this test case is very well suited to investigate the influence of the grid resolution (i.e. discretisation of the geometry, size of gradients) as well as the domain length (i.e. distance between the region of interest and the inflow and outflow) on the fluid mechanical results. In particular, if the computational domain is too short, the vortex shedding may severely be affected by the outflow boundary conditions.

Lattice Boltzmann methods are usually applied on an equidistant Cartesian mesh using the marker-and-cell approach which considers only two cell states: fluid or solid. Solid cells are blocked and therefore impermeable for fluid. Arbitrary geometrical shapes can be approximated on the lattice this way. The *bounce back* boundary condition allows a very efficient implementation of a no-slip boundary condition on the surface of the solid. However, the surface can only be described by a staircase approximation which resembles a *LEGO*-model. In the case of curved objects like a cylinder, this geometrical discretisation can have a large impact, especially on coarse grids at high Reynolds numbers. Recently, more advanced boundary conditions (e.g. *boundary fitting*) have been proposed for lattice Boltzmann methods which allow a much better description of the actual geometrical shape and surface. However, the computational effort of such boundary conditions is much higher and they tend to be less stable from the numerical point of view. Thus, the third aspect of this thesis is to test if better results (i.e. in particular more accurate results on coarse grids) can be obtained for low Reynolds number flows by using *boundary fitting* instead of *bounce back*. These results shall help to decide if it is worth or necessary to implement this sort of boundary condition into the actual production code *BEST* taking into account the effort of an efficient implementation and the much higher run-time costs compared to the standard *bounce back* rule.

For all investigations and the comparison with literature, the dimensionless vortex shedding frequency, the Strouhal number, is chosen. This quantity characterizes the time dependent flow behavior very well and can easily be determined from the wake.

1.3 Outline

This thesis is divided in the following sections:

- In chapter 2, the physical basics of the flow around a cylinder and the vortex shedding are summarized. This includes the definition of the characteristic dimensionless numbers (Re , St , C_D and C_L) and a description of the different flow patterns which occur with increasing Reynolds numbers. The influence of channel walls as well as the influence of the size of the computational domain are envisaged. At the end of this chapter, the historic evolution of the numerical simulation of the flow past cylinders from potential theoretical approaches to the numerical solution of the Navier-Stokes equations is shown.
- The lattice gas automata and the lattice Boltzmann approach are introduced in chapter 3.
- The investigated setup together with the applied boundary and initial conditions are described in chapter 4. Both, the *bounce back* and the *boundary fitting* boundary conditions model are described in detail. The procedure of determining the Strouhal number is also outlined in this chapter.
- In chapter 5, the calculated test cases are described. The results of the simulations are discussed and compared with literature.
- Finally, the results are summarized and an outlook to further investigations is given in chapter 6.

2 Vortex Shedding behind a Circular Cylinder

In this chapter the physical background of the flow around a cylinder and its characteristics are introduced. The dimensionless numbers referred to the problem are defined and the different flow regimes depending on the Reynolds number are described. The influence of channel walls and the influence of the size of the computational grid are summarized and at the end of the section some historic outlines of the development of the numerical simulations can be found.

2.1 The Relevant Dimensionless Numbers

The reason why alternating vortex detachments appear behind a thin body is the occurrence of instabilities in its wake. Those instabilities in impulse transport induce a process of periodic mutual displacement. Thus in a two dimensional flow behind bluff or round cylinders long vortex streets are formed. Below certain Reynolds numbers, which depend on the geometry, all instabilities are baffled by the molecular viscosity and no vortex street appears. Normally, for the description of a vortex street there are two dimensionless numbers used:

- Reynolds number

$$Re_\infty = \frac{U_\infty \cdot d}{\nu}$$

- Strouhal number

$$St_\infty = \frac{f \cdot d}{U_\infty}$$

The Reynolds number itself can be seen as a ratio of the characteristic length of the body, in our case the cylinder diameter d , multiplied by the free-stream velocity U_∞ and the kinematic viscosity ν .

The time-dependent behavior is described by the dimensionless Strouhal number, where f is the frequency of the oscillation of the transient flow and d and U_∞ , as in the definition of the Reynolds number, introduce the characteristic length of the object and the characteristic velocity. The Strouhal number can be considered as a dimensionless measure for the vortex shedding frequency.

Other important dimensionless numbers are the drag coefficient C_D and the lift coefficient C_L .

$$C_D = \frac{F_D}{1/2\rho U_\infty^2 d} \quad (1)$$

$$C_L = \frac{F_L}{1/2\rho U_\infty^2 d} \quad (2)$$

They are calculated from the sum of the viscous and pressure forces given by

$$F_D = F_{D\nu} + F_{Dp} = \int_S \mu \frac{\partial U_t}{\partial n_y} dS - \int_S P n_x dS \quad (3)$$

$$F_L = F_{L\nu} + F_{Lp} = \int_S \mu \frac{\partial U_t}{\partial n_x} dS - \int_S P n_y dS \quad (4)$$

where U_t is the tangential velocity and n_x and n_y are the x- and y- components of the normal vector to the cylinder surface S . The non-dimensional coefficients are obtained by normalizing the forces with the dynamic pressure.

The influence of the drag and lift coefficients can be seen in figure 1. In the attached and in the steady recirculating flow regimes, i.e. at $Re_\infty \leq 40$, the only force acting on the cylinder is the drag in the flow direction.

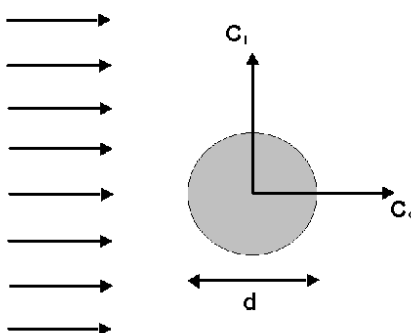


Figure 1: A two-dimensional presentation of the drag and lift coefficient acting on the cylinder

Finally, when there are confining walls, the flow development depends on a geometrical parameter, namely the diameter-to-width ratio or the so called blockage ratio

$$\beta = \frac{d}{H}. \quad (5)$$

Another point must be considered in case of confining walls. In a channel with laminar flow, after some time a parabolic velocity profile builds up. Unlike the free, unbounded flow where the value of the velocity in front of the obstacle is the same along the whole height of the domain (figure 2), here a maximum value is to be found in the middle and zero velocity at the channel walls (figure 3).

Previous works dealing with an object immersed in a flow confined by channel walls don't give an explicit answer to the question which velocity — the maximal or the mean one, should be taken into account when calculating the dimensionless numbers like Reynolds and Strouhal for instance. Zovatto and Pedrizetti [38] defined two different velocities, respectively two different Reynolds numbers: the Reynolds number of the channel — a

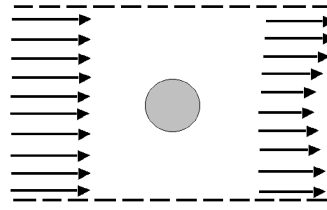


Figure 2: Profile of the free-stream velocity when there are no confining walls

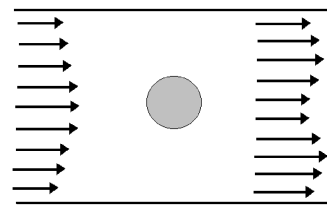


Figure 3: Profile of the velocity with confining walls

function of the average velocity in the channel, the channel height and the fluid viscosity and the cylinder-based Reynolds number where they used the mean velocity of the undisturbed parabolic flow profile at the height of the cylinder cross-section and the cylinder diameter (see chapter 5.6.6). Exactly the same did also Chen et al [6]. Kiehm et al [22], as well as Th. Zeiser [37] gave Reynolds number as a function of the average channel inlet velocity and the diameter of the cylinder. This last method is also favored and applied within this thesis, and our arguments are: if one takes the maximal velocity (i.e. the velocity in front of the parabolic profile) it yields lower values for the Strouhal number, which comply with the values found in literature for an unbounded domain, but the drawbacks of this approach would be, that the critical Reynolds number shifts up to quite high values: $Re_c \approx 80$ and higher. Yet, one should take into account the fact that a parabolic flow profile is set. Then it seems more plausible to use the mean velocity which can be read off after the simulations or take $\frac{2}{3}$ from the maximal velocity which should be equal to the value that can be read off. Because of the lower denominator in the formula for St in this case it will be higher than those found in other studies, but this is only due to the confinement of the flow.

2.2 Flow Regimes Behind a Circular Cylinder

It was already mentioned that the character of the flow depends on the Reynolds number, and for a cylindrical obstacle geometry there is a sequence of different Reynolds number ranges, in which different flow regimes occur. In the literature there is no clear division of

those regimes. In the flow visualization task in [10] there are five regimes presented, also by Graham [15] they are 5, but the most detailed dispartment can be found by Franke [12], who introduced seven regimes for the flow past a circular cylinder which are outlined below

- Flow past the cylinder without detachment, the so called Stokes flow for very small Re numbers

$$Re_{\infty} < 1$$



- Symmetrical detachment of the so called Föppl-vortex

$$1 < Re_{\infty} < 40$$



- Laminar vortex street

$$40 < Re_{\infty} < 150$$



- Transition from laminar to turbulent vortex street

$$150 < Re_{\infty} < 300$$



- Completely turbulent vortex street with laminar boundary layer on the cylinder

$$300 < Re_{\infty} < 300000$$



- Transition from laminar to turbulent boundary layer on the cylinder — completely turbulent wake without clear vortex street

$$300000 < Re_{\infty} < 3500000$$



- Turbulent boundary layer and completely turbulent wake with vortex street structure

$$3500000 < Re_{\infty}$$



For very low Reynolds numbers ($Re_\infty < 1$) the streamlines pass by the cylinder without forming any disturbances or irregularities.

By increasing the fluid speed, the flow changes gradually. For $Re_\infty > 1$ there is a recirculation behind the body. First it was thought that the recirculation grows continuously, but recently, it has been assumed that it appears suddenly, and it is certain that the recirculation length increases with Re . In any case, the character of the flow is different and a pair of vortices forms behind the cylinder.

The flow changes again by the time it gets to $Re_\infty = 40$. There is suddenly a complete change in the character of the motion. What happens is that one of the vortices behind the cylinder gets so long that it breaks off and sets off downstream with the fluid. Then the fluid curls around behind the cylinder and generates a new vortex. The vortices peel off alternately on each side, so that an instantaneous view of the flow looks roughly as sketched in the third figure above. The stream of vortices is called a “von Karman vortex street”.

There is a complete difference in the flow patterns in the third figure compared to the first two figures. While in the first two the velocity field is static, the velocity for $Re_\infty > 40$ at any point varies with time. For these higher Reynolds numbers there is no steady state solution, but the time-dependent oscillation of the flow follows a regular, cyclic fashion.

As the velocity increases further there is less and less time for the vorticity to diffuse into a larger region of the fluid. By the time we reach $Re_\infty = 150$ the vorticity begins to fill in a thin band. The region is called boundary layer and this irregular flow region, where the fluid is subject to shear forces, works its way upstream as Re is increased.

In the turbulent region, the velocities are very irregular and noisy; also the flow is no longer two-dimensional but twists and turns in all three dimensions. There is still a regular alternating motion superimposed on the turbulent one.

As the Reynolds number goes up, the turbulent region works its way forward until it reaches the point where the stream lines leave the cylinder. Thus the turbulent boundary layer is set. Also there is a drastic change in the drag force; it drops by a large factor. In this region the drag force actually decreases with increasing velocity and there seems to be little evidence of periodicity.

Further on, experiments which go up to Reynolds numbers in the range of 10^7 indicate that a new periodicity appears in the wake, either because the whole wake is oscillating back and forth in a gross motion or because some new kind of vortex is occurring together with an irregular noisy motion.

The itemization of the Reynolds number regimes for the circular cylinder shows, which importance the implementation of the turbulence can have for the development of the total flow. But in this work we consider only the laminar, time-dependent case.

2.3 Influence of the Computational Domain on the Flow

For the design of the computational domain and grid it is important to consider some details at this point. In general, for the calculations of the different flow regimes two different types of computational domains and grids have to be employed (circular and rectangular) in order to achieve reasonable output: one for the lower and one for the larger values of Re . For all simulations at very low Reynolds numbers ($Re_\infty < 1$), the computational domain has to be extremely large and adjusted to the actual value of Re . The use of a circular domain is advantageous in this case. Because the region of the flow disturbed by the cylinder at low values of Re is of similar magnitude in front and at the rear of it. For Reynolds numbers larger than about 1, a pair of standing vortices appear at the rear of the cylinder, demanding a finer discretization of that region. And for laminar vortex shedding flow regime at moderate Reynolds numbers ($Re_\infty > 40$) the computational domain has to be elongated downstream in order to capture correctly the von Karman vortex street. On the other hand the cylinder disturbs a smaller region in the front and lateral directions compared with the other regimes. Therefore a different type of domain, a rectangular domain has to be adopted for this range of Reynolds numbers.

Another item that should be taken into account is that if the boundary of the computational domain does not approximately accompany the expansion of the influence region at smaller Re numbers, the error caused by the artificial boundary condition disturbs the solution, affecting even the vicinity of the cylinder.

The present work, being a two dimensional simulation of a flow around a cylinder, allows calculations only for a laminar flow, which means $Re_\infty < 150$. In this case a rectangular channel with dimensions much larger than those of the cylinder itself has been chosen. As the flow in a confining box is investigated, the lateral dimension is fixed by the blockage ratio and only the length of the domain is variable. A special study devoted to the question how big the influence of the length of the domain and the size of the obstacle (section 5.2 and 5.3) is, was carried out in order to obtain an optimal geometrical configuration.

2.4 Influence of Confining Walls

In many studies from the beginning of the 20 century till the present days the unbounded flow domain introduces difficulties in the analysis from the theoretical and numerical points of view. The reason why numerical studies regarding confining walls are carried out is that for a flow which is unbounded in all directions, the truncation of the flow domain is inevitable in any numerical simulation. However, this will pose many difficulties, mainly because there are only partial estimates for the decay of solutions of the Navier-Stokes equations at large distances. Accordingly, there is no way of knowing how to truncate the flow domain for computational purposes so as to provide a provable approximation of the flow in the unbounded domain. Secondly, since all experiments must be carried out in experimental facilities of finite size, no theoretical or computational investigation can be

compared with experimental investigations. In addition the confined flow is of importance for many technical applications as shown in the introduction.

All the data from the experimental investigations done by Grove et al. (1965) [16], Acrivos et al. (1968) [1], Coutance and Bouard (1977) [8] and Smith (1979) [28] show that the stability of the steady wake is greatly enhanced by the increase of the blockage ratio, since the wake instability is caused primarily by the disturbances which are generated in a direction perpendicular to both that of the undisturbed flow and the axis of the cylinder. Thus it appears reasonable that the propagation of such disturbances should be inhibited by the presence of the walls which confine the streamlines near the cylinder. Acrivos made experiments with Reynolds numbers lower than 150 and blockage ratios 0.025 and 0.05, Coutance and Bouard worked in the range $5 < Re < 40$ and with blockage ratios $0.024 < \beta < 0.12$ and both studies yielded results which agree with Grove's observations, that the eddy length varies nearly linearly with the blockage ratio.

As for numerical studies, the problem of estimating the onset Reynolds number for separation has not yet been carefully and systematically investigated. Numerical studies were done by Fornberg (1980) [11] and Chen (2000) [7]. The results from Chen, just like those from Fornberg, once again confirmed the theoretical arguments put forward by Smith, namely that the elongation development of the recirculating region linearly follows the Reynolds number.

2.5 The Numerical Simulation of Vortex Streets — a Historic Overview

With the increasing efficiency of the available computer systems the simulation of in-stationary periodic flow became possible within realistic processing time. In contrast to experimental measurements, the numeric approach allows a relatively simple access to the complete velocity and pressure fields and thus a detailed analysis of the flow process. The main problems of numerical methods is above all the question of the accuracy of the solution and the numerical stability, moreover only idealized boundary conditions, especially at the outlet of the flow can be predetermined.

Because of the practical importance of the periodic vortex detachment, in the last years there were taken pains to predict those flow regimes. The variation width of the techniques applied for this purpose has been summarized by Celik (1986) [5]. The described approaches can be divided in two classes:

- The numerical solution of the potential theoretical approach considering the interactions with empirically brought-in viscosity influences and discrete vortices (discrete vortex methods)
- The numerical solution of the Navier-Stokes equations
 - a) in the time-averaged form
 - b) in the time-dependent form

In the discrete vortex methods by means of a Lagrange approach the transport of rotating afflicted fluid elements (discrete vortices) over the Biot-Savart law is determined. The flow velocities are then determined from a potential theoretical approach, in which the influence of the discrete vortices shrinks. The biggest disadvantage of this process is the necessity that the discrete vortices should be brought in the flow field by the use of empiric information explicitly at the point of detachment. Since the position of the point of detachment and the vortex powerfulness depend on the geometry and the Reynolds number, the universality of the approach is limited.

Methods, which can numerically solve the complete, non-linear Navier-Stokes equations and the continuity equation are preferred because of their wider range of application. This technique was applied already more than 30 years ago for the periodic flow past cylinders by Son and Hanratty (1969) [29], but still nowadays there are studies which deal exclusively with two-dimensional vortex street at low Reynolds numbers and don't take into account the stochastic functions. For a spatial two-dimensional computation the equations are either formulated in primitive variables (u, ν, p) or by means of the stream function and the rotation.

3 Introduction to the Lattice Boltzmann Approach

This chapter gives a brief introduction to lattice gas and lattice Boltzmann methods. More information on the subject including details of the mathematical derivations can be found e.g. in J. Bernsdorf [2], J. Buick [4], D. Hanon and O. Tribel [17], F. Huber [19] and Kohno [23].

3.1 The Development of Lattice Gas Automata

The first model of Lattice Gas Automata (LGA) was invented in 1973 by Hardy, Pomeau and de Pazzis [18] (it is thus called “HPP”-model), in order to study ergodicity-related problems. These systems being entirely discrete present the advantage of a straightforward implementation on computers and they allow to perform simulations with many more particles than “realistic” models in which one has to take into account the continuous values of positions, velocities and interaction potentials with finite precision.

The HPP-model is based on a square lattice whose nodes can be occupied by the “fluid”’s particles. Thus space is discretized, and in practice it is also finite. The boundary conditions are usually chosen periodic. In addition, momentum is also disturbed in discrete fashion: all particles have the same mass (equal to one unit) and equal absolute velocity also equal to one unit, i.e. they will fly from one lattice node to the nearest neighbor in one unit of time (thus time is absolutely discrete). Furthermore, an exclusion principle is imposed on the particles for numerical efficiency reasons, i.e. no two particles may sit simultaneously on the same node if their direction is identical. On the HPP’s square lattice this implies that there can be at most four particles per node.

The interactions between the particles are simple: they may only take place on nodes with several particles, taking the form of local instantaneous collisions. The collision rules are chosen in order to conserve both mass and momentum. In this model there is no additional conservation law associated to energy since energy is directly proportional to mass; it is thus trivially conserved.

The evolution of the system from one time-step to the next takes place in two successive stages:

- propagation: the particles move from their node to the nearest neighbor in the direction of their velocity vector
- collision: particles on the same node may exchange momentum if it is compatible with the imposed invariance-rules.

It was quickly realized though, that HPP presents only limited applications. The underlying reason for this is that the lattice is based on a very limited symmetry-group of order four. This leads to macroscopically anisotropic Navier-Stokes equations. It was

proved that this main defect does not appear when using a lattice with triangular cells and hexagonal symmetry.

That was the main consideration leading to the birth of the FHP-model (invented by Frisch, Hasslacher and Pomeau [13]) in the mid-eighties. The basic ideas are the same as those underlying the HPP-model, but the lattice's symmetry group of order six offers greater wealth. First of all, the FHP's Navier-Stokes equations make microscopical hydro-dynamical simulations possible, both in laminar and turbulent flows, and in an environment which can easily be controlled. Moreover, the number of effective collisions is much greater than what was available by the HPP-model, which affects the viscosity of the fluid.

Sure enough, the lattice gas model family has also been extended to simulate three dimensional hydrodynamics. The fact that there is no three dimensional lattice with sufficient symmetry to lead to isotropic Navier-Stokes equations requires a short detour in the fourth dimension: the projections of a "slide" of a lattice formed by tesseracts ("four-dimensional cubes") into three dimensional space does the trick. The model is called FCHC-model ("Face Centrated Hyper-Cubic" lattice) and has been validated both by theory and by numerical experiments.

3.2 The Background of the Microscopic Model of Fluids

Using kinetic theory we are able to predict macroscopic characteristics of a fluid on the basis of a detailed microscopic description of the distribution of speeds of individual molecules and a set of approximations about how individuals interact. There are a few obstacles concerning the description of the behavior of the macroscopic fluids. One main problem is the complexity of interactions and another is the huge number of molecules, which have to be considered. Therefore, the real micro-world cannot be used for solving usual configurations.

To allow an efficient simulation of the macroscopic behavior, the real micro-world has to be replaced by an effective model as simple as possible which still leads to the same macroscopic behavior. The basic idea is that all details of the microscopic interactions are not relevant for the overall behavior. Thus it is sufficient to use a model with much less particles and simple interaction/collision rules. The particle movement can take place on a regular lattice. The most important feature of the collision rules — which may be purely local — is that they conserve mass and momentum, because these are also the quantities which are of interest in the macroscopic limit.

Thus it is possible to construct a very simple model which efficiency runs on computers. This artificial system may be called cellular automata [34].

The transition from the micro-world to the macro-world consists in ensemble averaging. This step is the same for the real micro-world and the simplified model. It consists of calculation average distribution probabilities over large enough spatial areas or long enough time periods to give noise-free values of ρ and \vec{u} .

As mentioned above the particles in the model system have unit mass and move in discrete time steps with unit velocity in one of the few directions. The movement is described in a dimensionless form: the unit length l_u is the distance between two neighbor nodes, i.e. the diagonal and the time t_u is defined as the time interval a particle has to move from one node to a neighbor node ($= l_u$). Consequently, the particle or lattice velocity e_i has the value 1

$$x = l/l_u \text{ and } t = t/t_u \rightarrow e_i = x/t = (l/t) * (t_u/l_u) \quad (6)$$

in the time t_u the particle moves the distance $l = l_u \rightarrow e_i = 1$.

To summarize: the difference between a real gas and a lattice gas model consists of the following:

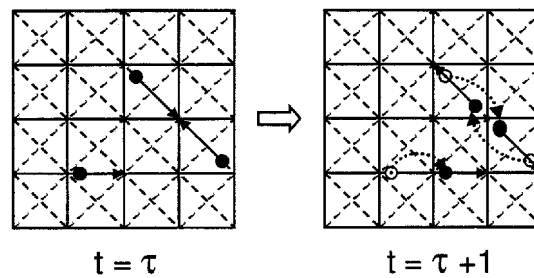
- The particle density on the lattice is by scales smaller than the one in real gas, which contains about 10^{19} molecules per cm^3 .
- The use of particles with unit mass, whereas a real gas can include different masses, if different molecular types are present (e.g. in a gas mixture).
- A real gas also shows a velocity distribution affecting a continuous momentum distribution. Lattice gas particles have unit velocity and move only in the directions of the lattice links. Therefore, they have a discrete momentum.
- Finally, advection and interactions in a real gas are random. In a lattice gas the particles move and collide in discrete time steps until the system converges, that means until the macroscopic quantities (like local fluid density) determined from the model vary slightly around a constant value for the given conditions. In this way, lattice gas simulations are an iterative process.

Despite the simplifications such automata provide reasonable results, because details of the microscopic interactions are not relevant for fluid dynamic simulations.

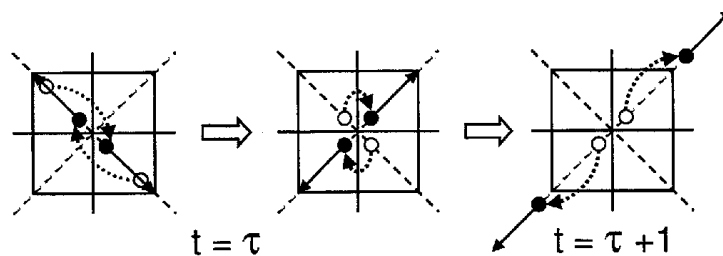
3.3 The Lattice Gas Algorithm

As mentioned before, a lattice gas simulation is an iterative process solving the time evolution of the fluid. At each time step an algorithm composed of three main steps is performed. In the following an octagonal lattice is assumed — but without loss of generality.

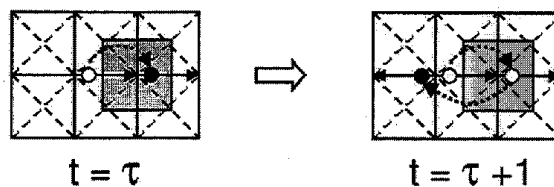
propagation: per time step, the particles propagate along one of the eight possible directions from one cell to its next neighbor cell according to their lattice vector. This process is called advection or propagation.



collision: if well defined particle configurations occur, collisions take place. The particles exchange momentum while conserving the total mass and momentum at each node. The microscopic interactions are strictly local because they involve only particles at a single node.



wall boundary conditions: boundaries and obstacles can be introduced into the model by initially labelling certain lattice cells (marker-and-cell approach). Thus any geometrical structure can be depicted. Different collision rules are then applied at these cells. No-slips are introduced at a boundary by forcing any particle colliding with the boundary to return along the link on which it approached.



The micro-dynamics consist of a repetition of propagation, collision and bounce back and this loop is iterated until an equilibrium state is reached that means for steady systems conditions until the local macroscopic quantities reach a constant value. In this case of time-dependent flows, each iteration gives the results of the next time step. In any case the macroscopic quantities (like \vec{u} , ρ) can always be calculated from the particle distribution by the so-called ensemble averaging or coarse graining.

3.4 The Lattice Boltzmann Approach

The big advantage of LGA is the simplicity of the algorithm. But using discrete/boolean occupation states (i.e. particle is present or not) leads to large statistical noise which

requires averaging over large areas or many time-steps to get smooth macroscopic variable changes. These drawbacks no longer exist in the LBA while the simple algorithm is kept.

3.4.1 From Lattice Gas to Lattice Boltzmann

The lattice Boltzmann approach has evolved from the lattice gas models. Various modifications have been made to overcome the difficulties with the lattice gas approach to fluid modelling, but using its advantages. Unlike the lattice gas, the LB does not use binary particles. Instead of particles, the model deals with continuous particle density distribution functions. These density distributions represent the probability to find particles on a single node moving in a certain direction. In the dimensionless form, they can be continuous values between 0 and 1. Thus the macroscopic values change smoothly without averaging. The distribution functions interact again locally, i.e. only distributions at a single node are involved. After “collision” they propagate to the next neighbor node.

As a second point, the collision process can be simplified. The Boltzmann equation (BE), the basis of LB, describes the motion and interaction of fluid particles, by using a single particle distribution function f .

$$\frac{\partial f}{\partial t} + \vec{\xi} \frac{\partial f}{\partial \vec{x}} + \vec{F} \frac{\partial f}{\partial \vec{\xi}} = \Omega(f) \quad (7)$$

with $\vec{\xi}$ = microscopic particle velocity
 \vec{F} = body force per unit mass and
 $\Omega(f)$ = collision integral

The Boltzmann equation is an approximation of the real fluid. The collision integral considers only 2-particle collisions. Furthermore the particle velocities are assumed to be uncorrelated before collision.

3.4.2 Discretization of the Boltzmann Equation

In order to get an equation applicable for computational simulations, the BE has to be discretized: the velocity space is discretized by introducing a finite set of discrete velocities \vec{e}_i and associated distribution functions $N_i(\vec{x}, t)$ and in a second step, time and space are discretized.

This leads to the so-called lattice Boltzmann equation, which is the equation of the LB method.

$$N_i(\vec{x} + \vec{e}_i \cdot \Delta t, t + \Delta t) = N_i(\vec{x}, t) + \Omega_i \quad (8)$$

where the left side represents the propagation; $\vec{x} + \vec{e}_i \cdot \Delta t$ refers to the next node; $t + \Delta t$ the next time step; \vec{x} is the local node, t the current time and Ω_i is the collision operator. Still the collision integral is a problem. It has a very complicated structure, therefore alternative, simpler expressions have been proposed. The idea behind the replacement is

that the large amount of detail about 2-body interactions is not likely to influence the values of many experimentally measured local macroscopic quantities significantly, i.e. no detail information about the particle interactions are necessary [35].

3.4.3 BGK Relaxation

The most widely known collision model is the BGK approximation named after their authors. Here, the collisions are not explicitly defined, but they are kind of fictive. The idea is to simplify the collisions as a relaxation process towards the local equilibrium state expressed by equation (9). The BGK approach can be written in the continuous form with f as well as in the discretized form with N_i .

$$\Omega_i = \omega[N_i^{eq}(\rho, \vec{u}) - N_i(\vec{x}, t)] \quad (9)$$

with ω = relaxation parameter

N_i^{eq} = Maxwell-Boltzmann distribution function (MB) (equilibrium density distribution)

N_i = discretized distribution function.

The concept of this approach is that the collisions at a certain space point and time instant change the distribution function N_i at that point by an amount proportional to the departure of N_i from the Maxwellian equilibrium distribution. The physical motivation is that each system tries to reach its equilibrium state. The local equilibrium state for the considered flow systems is given by the Maxwell Boltzmann distribution. The collision frequency (which gives the viscosity of the fluid) determines how fast this occurs.

For computational simulations using the Lattice Boltzmann equation with the BGK approach, the Maxwell-Boltzmann equilibrium distribution has to be discretized in the velocity space by a Taylor expansion. In order to describe the correct hydrodynamic behavior of the fluid, the velocity terms up to 2^{nd} order have to be taken into account.

$$N_i^{eq} = t_p \cdot \rho(1 + 3 \cdot \vec{e}_{i\alpha} \cdot \vec{u}_\alpha + \frac{9}{2} \vec{u}_\alpha \cdot \vec{u}_\beta (\vec{e}_\alpha \cdot \vec{e}_\beta - \frac{1}{3} \delta_{\alpha\beta})) \quad (10)$$

with t_p — lattice direction dependant constant

\vec{u} — macroscopic velocity

$\alpha, \beta : \{x, y, (z)\}$ — component of the local lattice link; Einstein summation applied over repeated indices

$i = 0 \cdot \cdot N$ — index of the local lattice link

and $\delta_{\alpha\beta}$ — Kronecker-Delta operator.

3.4.4 Numerical Application of the Lattice Boltzmann Approach

Now, the lattice Boltzmann equation using the BGK approach can be applied for computational simulations. For a given space point and time step this equation consists of the same simulation steps as the algorithm of the lattice gas model.

- The relaxation step with the BGK approach reflects the influence on the distribution function due to collision, i.e. the particle distribution changes according to the relaxation rule. This step replaces the collision step in LGA.
- After the collision the particle distribution propagates along its associated link to its next neighbor node. The direction is again determined by the lattice vector. This step is the same as in LGA.

The transfer of the microscopic states to the macroscopic level is easy.

density $\rho(\vec{x}, t) = \sum N_i(\vec{x}, t)$

velocity $\vec{u}(\vec{x}, t) = \frac{\sum N_i(\vec{x}, t) \cdot \vec{e}_i}{\rho(\vec{x}, t)}$

viscosity $\nu = \frac{1}{6}(\frac{2}{\omega} - 1)$

pressure $p = \rho \cdot c^2$

Like the lattice gas model, the LB simulation describes the time evolution and the microdynamics consists of a repetition of local relaxation and propagation. It can be applied to a variety of science and engineering fields including highly complicated fluid dynamic phenomena like multi-phase flow, turbulent flow, internal flow in complicated structures, etc.

4 Evaluation of the Vortex Shedding in a Channel

In this chapter the boundary and initial conditions are introduced, whereas the algorithm of two types of boundary conditions — the *bounce back* and the *boundary fitting* approaches are described. The range of investigated Reynolds numbers as well as the evaluation of the detachment frequency and determination of the Strouhal numbers are explained in detail.

4.1 Investigated Reynolds Numbers

Considering the fact that the periodic detachment starts at $Re_\infty = 40$ for the unbounded flow or higher for confined flow, values between $Re_\infty \approx 60$ and $Re_\infty \approx 210$ have been chosen for the computations. As already discussed in section 2.1, the characteristic velocity (and length) can be defined in several different ways if channel walls are present. As we decided to use a Reynolds number based on the cylinder diameter and the mean channel velocity, the rescaled Reynolds number range is $Re_{mean} = 41$ to $Re_{mean} = 146$. The correct definition of the Reynolds number (and the Strouhal number) must always be considered when comparing with data from literature. Commensurable experimental data can be found in section 5.6 where this point has carefully been taken into account.

In the numerical simulation once the obstacle size is defined, there are only two parameters to be set to obtain the Reynolds number — the inlet velocity and the viscosity. The Reynolds numbers are manually incremented by decreasing the viscosity, i.e. simultaneous increasing of the relaxation parameter ω .

By all simulations, the following procedure was applied: the channel parameters (length, height and blockage ratio), the obstacle size and the desired range for the Reynolds number were chosen. On the basis of these Reynolds numbers the kinematic viscosity, respectively the relaxation parameter were computed and specified in the parameter file along with the maximal inflow velocity $U_{max} = 0.05$. After running the simulations the detachment frequency used by the determination of the Strouhal number and the actual mean velocity in the channel, which is around $\frac{2}{3}$ of the specified one, are read off.

After evaluating the results, it turned out that the actual value of the mean axial velocity lies in the interval between 0.0340 and 0.0347 instead of being exactly $\frac{2}{3} \cdot 0.05 = \frac{1}{30}$. This slight deviation is due to way the inlet boundary condition is implemented (see below). In the calculation of the Strouhal number, this measured effective mean velocity is used and the corresponding Reynolds number is corrected a posteriori.

Normally low velocity values are desired, because in lattice Boltzmann automata, the approach error increases with the square of the Mach number

$$Ma = \frac{U}{c} \quad (11)$$

where c is the sound velocity. On the other hand, low velocities lead to a long period of the vortex shedding as can be seen from equation (12). Thus to avoid too long computational

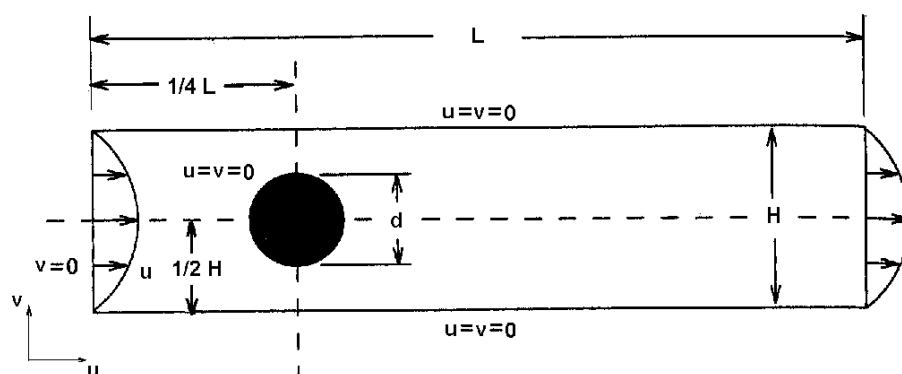


Figure 4: Scheme of the channel

durations a compromise between the computational effort and the Mach number error must be made. In the present case, the Mach number is below 0.09 so that any error introduced by the Mach number approximation can safely be neglected.

$$T = \frac{D}{St \cdot U} \quad (12)$$

The velocity is indirectly proportional to the period duration. Thus the number of iterations must increase with the same factor as the velocity decreases if one wants to retain the same number of periods because the time step Δt is fixed in the lattice Boltzmann approach.

4.2 Schematic Presentation of the Channel

The computational domain is presented in figure 4, though in the different investigated cases the Reynolds number, the obstacle size and the distance between the obstacle and the boundaries of the computational domain vary. The center of the obstacle lies invariably horizontally at $\frac{1}{4}$ of the length of the computational domain and vertically in the middle of it. The exact specification of the different lengths can be found in the sections where the different results are discussed (tables 1 to 5). In general, the blockage ratio varied between 0.1 and 0.4. The length L of the domain was set up to 160 diameters leading up to 102×1600 voxels.

4.3 Boundary and Initial Conditions

The upper and lower boundary of the computational domain consist of the channel walls. There, as well as on the surface of the cylinder, a no-slip boundary condition is applied which ensures that both components of the velocity are zero. Depending on the program version used, bounce back or boundary fitting are used. Details on these boundary conditions are given later in section 4.5.

At the inlet a parabolic velocity profile is set using the maximal velocity U_{max} . In lattice Boltzmann methods the specification of the pressure and the velocity is not sufficient, because not they, but the particle density distribution is saved on the nodes. That is the reason why at the inlet the macroscopic density is extrapolated from the cells downwards and along with the specified macroscopic flow velocity they are used to calculate the according equilibrium distribution by applying the formulas:

$$N_0^{eq} = \frac{4}{9}\rho(1 - \frac{3}{2}u^2) \quad (13)$$

$$N_i^{eq} = \frac{1}{9}\rho(1 + 3c_i \cdot u + \frac{9}{2}(c_i \cdot u)^2 - \frac{3}{2}u^2) \quad \text{for } i = 1, 3, 5, 7 \quad (14)$$

$$N_i^{eq} = \frac{1}{36}\rho(1 + 3c_i \cdot u + \frac{9}{2}(c_i \cdot u)^2 - \frac{3}{2}u^2) \quad \text{for } i = 2, 4, 6, 8 \quad (15)$$

At the outlet from the cells upwards the flow the velocity is extrapolated and together with the fixed pressure it is used by the calculation of the equilibrium distribution. Particle density distributions that reach the inlet and outlet cells by propagation are not considered any further and at each iteration overwritten by the calculated equilibrium distribution.

Using the equilibrium distribution function in the inlet and outlet row introduces a small deviation of the effective values from the desired ones. As a result, the actually obtained inlet velocity is not exactly the one which is set. The difference depends on the relaxation parameter (the speed with which the equilibrium is approached within the flow) as already mentioned in section 4.1.

As initial condition $\vec{u} = 0$ and $p = const$ at $t = 0$ is chosen. This solution is correct from the fluid mechanical point of view and can correctly be expressed in terms of the equilibrium distribution function. Then a "pump" is smoothly turned on by slowly increasing the axial inflow component (the transversal component is always 0) and increasing the relaxation parameter in the form of a sine-function over a few thousand iterations.

4.4 Evaluation of the Detachment Frequency

In order to determine the detachment frequency one cell in our computational domain was selected and the time evolution of the v-velocity was observed. Figure 5 shows this temporal evolution.

For the evaluation of the obtained data, the power density spectrum of the v-velocity is calculated. For this purpose the autocorrelation and Fourier transformation functions of the visualizing tool *xmgr* are applied. The result of the two transformations is the power density spectrum. Since the Fourier transformation is in the range between $(-\infty; \infty)$, but in practice only a discrete number of data is available, through the spectral analysis only discrete frequency information is obtained. In order to increase the resolution it's not enough to increase the sampling frequency to enlarge the sample length. The number of independent data values — that is the observation duration, is much more important. The

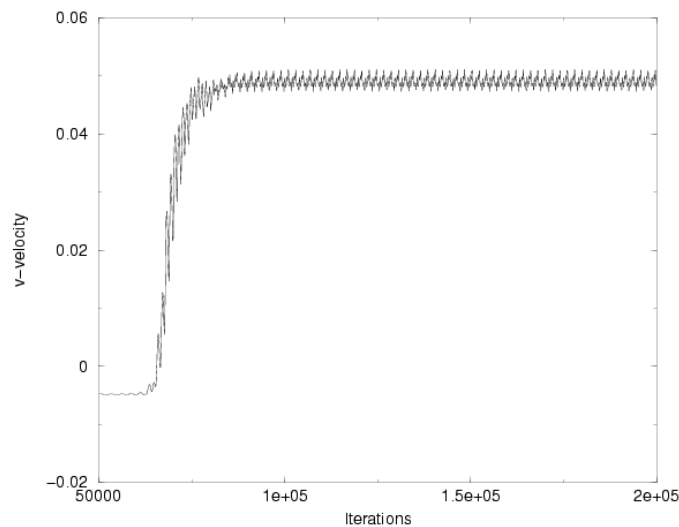


Figure 5: Development of the v-velocity in the point with coordinates $x = \frac{L}{2}$ and $y = \frac{H}{2} + 0.5$ in a coordinate system based on a cartesian coordinate system starting in the low left corner of the computational domain. $Re_{mean} = 131.9$, $\beta = 0.2$.

minimal necessary sampling rate $f_s = \frac{1}{T}$ at which still no information gets lost, is given by the sampling theorem. This theorem states that for a limited bandwidth (band-limited) signal with a maximum frequency f_{max} , the equally spaced sampling frequency f_s must be greater than twice of the maximal frequency f_{max} , i.e.,

$$f_s > 2f_{max}$$

in order to have the signal be uniquely reconstructed without aliasing. Each periodic length should acquire at least 2 points. If in the spectrum even greater frequencies appear, those won't be recognized and through aliasing improperly appear at smaller frequencies.

In all investigated test cases, every 100 iterations were chosen to be sampling time points independently of the obstacle or grid size. The sampling theorem is fulfilled, since the vortex detachments are expected to appear by frequency smaller than $\frac{1}{1000}$ iterations.

Evaluating the detachment frequency, there's one phenomenon that draws one's attention. After applying the autocorrelation and Fourier transformation tools of *xmgr* one expects to obtain just a single peak in the power density spectrum of the v -velocity, which value of the axial coordinate would give the most frequently recurrent detachment frequency. As a matter of fact in all cases of the present study, there were three or more peaks of a different height (see figure 6 and figure 7). Nevertheless, always the first peak supplies us with the most reasonable values for the detachment frequency and Strouhal number and the following peaks are nothing but its superharmonics (i.e. multiples of the frequency of the first peak).

With the help of a few numerical experiments it could be demonstrated that the height of the peaks depends on the y -coordinate of the cell in which the v -velocity is measured. The further the cell is from the middle of the channel, the higher the first peak is. Two cases

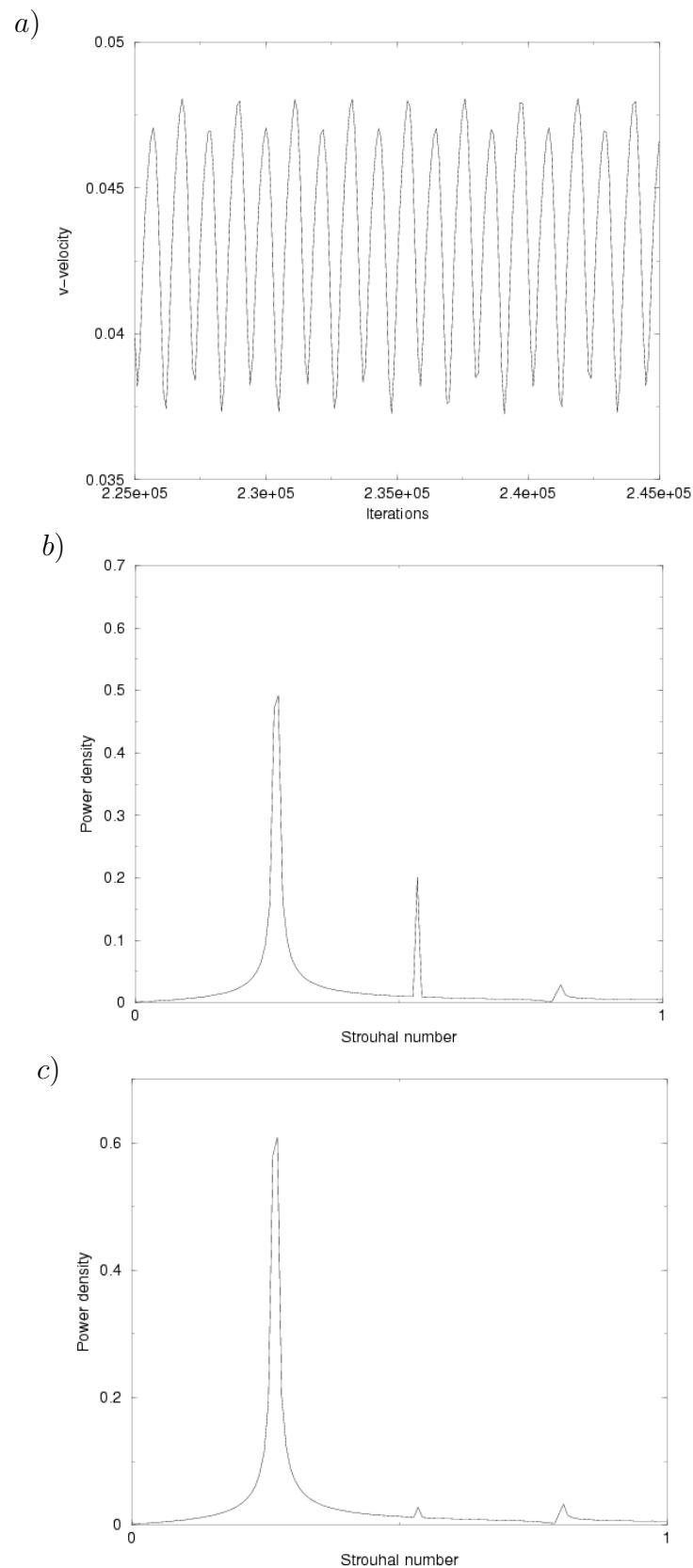


Figure 6: A closeup look at a) the v -velocity and b) and c) the power density spectrum plotted against the Strouhal number for $\beta = 0.2$ and $Re_{mean} = 83.3$. In b) the marked cell from which the evolution of v -velocity was observed was placed vertically about $\frac{H}{10}$ from the middle of the channel and in c) the distance is about $\frac{H}{5}$. Although in the power density spectrum three separate peaks of different height can be recognized, the value for St is always yielded from the first one

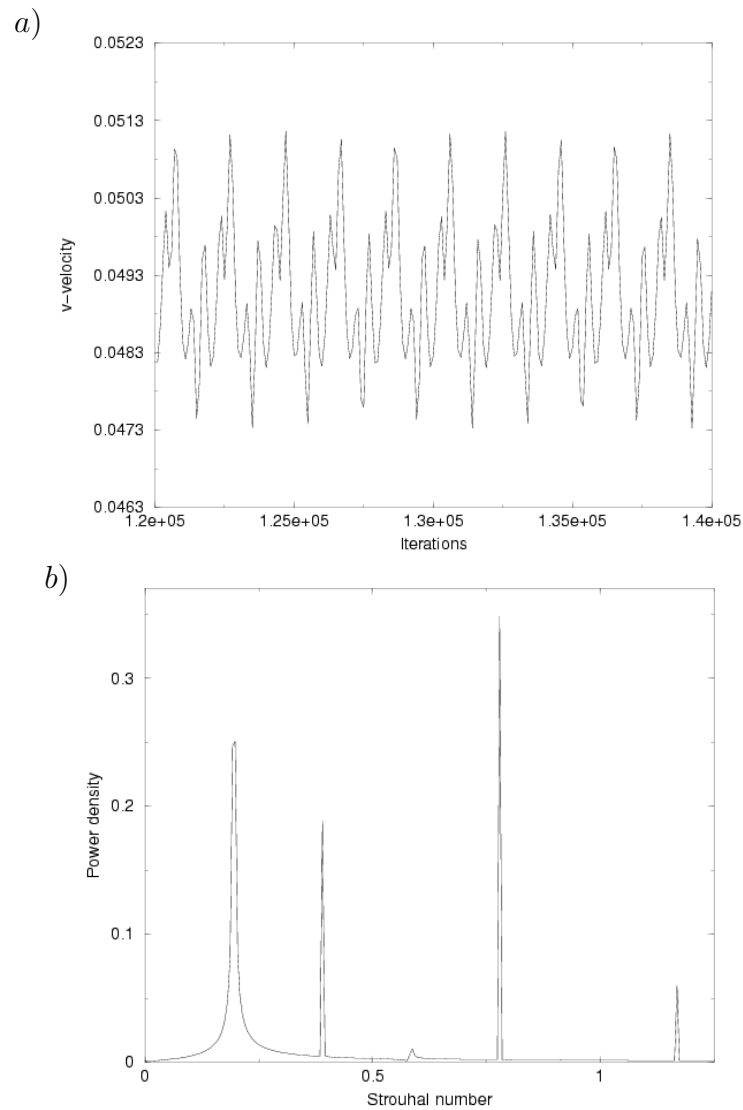


Figure 7: A closeup look at a) the v -velocity and b) the power density spectrum plotted against the Strouhal number for $\beta = 0.2$ and $Re_{mean} = 131.9$. The cell from which the v -velocity was measured lied in about the middle of the channel, that's the reason why the first peak is not the highest in this presentation. The coexistence of more peaks is due to the fact, that additional detachment modes at high Reynolds numbers cause additional disturbances. Again the Strouhal number is read off from the very first peak.

were tested — when this cell lies vertically about $\frac{H}{10}$ away from the middle of the domain, and when the distance is about $\frac{H}{5}$. By means of the results presented in figure 6 b) and c) we can draw a conclusion that the case of $\frac{H}{5}$ is the optimal one. Therefore it seems that closer to the channel wall only the primary detachment is seen whereas in the center different vortices overlay and secondary effects occur leading to strong superharmonics.

4.5 Boundary Fitting Versus Bounce Back Boundary Conditions

The usual boundary condition for solid walls in *LBA* is the bounce back boundary condition. The no-slip condition is achieved here by reversing all particles or particle distributions hitting a wall to their original cell with opposite direction/momentum. The advantage of this boundary condition is its simplicity. But the position of the wall surface is always halfway between the cells. Thus, the real geometrical surface can only be approximated by a staircase surface, like a *LEGO* model.

In recent years, more advanced boundary conditions have been proposed. In this work, the boundary conditions of Bouzidi et al. (2001) [3] will be investigated. With this boundary condition, the surface of the solid wall can be placed at any position — not just halfway between the cells. The basic idea of this enhanced boundary conditions is to consider the exact position where the surface cuts the links. In cells next to a wall some directions are not updated by the normal propagation step. In the boundary fitting algorithm of Bouzidi, some distribution value (before or after propagation) is interpolated from the two cells next to the wall and after "advection", this population reaches the position of the "missing information". In figure 8 the two possibilities which depend on the distance between the last fluid cell and the intersection point (link-solid surface) are depicted for 1D case.

The location of the wall is given by $q = \frac{|AC|}{|AB|}$ where A is the last node before the wall, B is the first node behind it (i.e. in the wall) and C is the point where the solid surface intersects the link. A particle leaving A and reflecting on the wall will not reach a fluid node after moving with velocity 1 over a total distance 1 except if q is equal to 0, $\frac{1}{2}$ or 1, thereby $q = \frac{1}{2}$ is identical with the normal bounce back boundary conditions. This means that after the collision step the population of particles at A with velocity -1 is unknown. The following scheme was proposed:

- for $q < \frac{1}{2}$ from the available information in the fluid the population of fictitious particles at location D that will travel to A after bouncing back on the wall at C is constructed.
- for $q \geq \frac{1}{2}$ the information on the particle leaving A and arriving in D together with the new postadvection situation at fluid nodes E and F will be used to compute the unknown quantities at A .

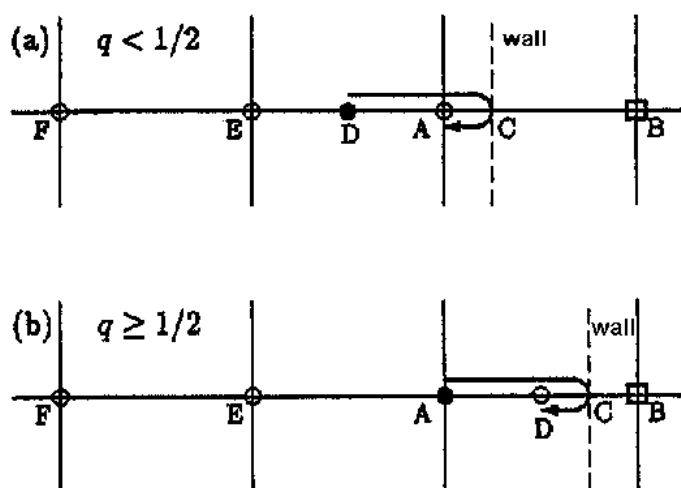


Figure 8: The boundary-fitting model applied by the collision of the particles at a wall

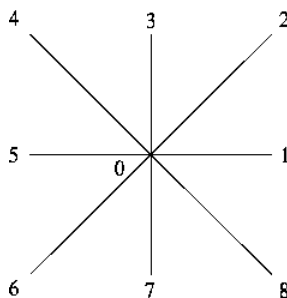


Figure 9: Octagonal lattice cell

To use this enhanced boundary conditions for the present configuration of a circular cylinder, the exact intersection positions must be known. The determination of these points is not as trivial as it might seem at first glance as all 8 directions of a $D2Q9$ must be considered (see figure 9). The following algorithm is applied to get the positions and distances. All cells which satisfy condition 16 are within the solid.

$$(x_* - x_{center})^2 + (y_* - y_{center})^2 < R^2 \quad (16)$$

x_* and y_* denote the coordinates of the lattice cells and thus they can only be integer values whereas the center of the cylinder x_{center} and y_{center} as well as the radius R can be floating point numbers.

To obtain the exact intersection positions, the equation of a circle has to be solved for the different lattice lines.

For the horizontal direction, the following equation is solved

$$R^2 = (x_* - x_{center})^2 + (y_* - y_{center})^2 \quad (17)$$

which gives two values of x for each $y_* = const.$

The distance between x and the closest x_* in the fluid domain is stored and used as q during the boundary fitting advection step as described above.

A similar equation also results in the vertical direction.

The inclined lattice lines are defined by

$$y = x + k \quad (18)$$

$$y = -x + k \quad (19)$$

where k is the offset of the lines and k lies in the interval $[(x_{center} - y_{center}) - (\sqrt{2}R + 1); (x_{center} - y_{center}) + (\sqrt{2}R + 1)]$ for the lines with positive slope and in the interval $[(x_{center} + y_{center}) - (\sqrt{2}R + 1); (x_{center} + y_{center}) + (\sqrt{2}R + 1)]$ for the lines with negative slope. x and y can now both be floating point numbers but k is always integer. Again, the two intersection positions for each k are determined from the equation of the circle and the distance from the closest fluid node to the exact intersection point is stored for further use.

By considering the intersection of the real geometry with the lattice links, inclined and curved surfaces can be represented very well. Figure 10 compares the resulting geometry using boundary fitting and bounce back. Each small square represents the center of a cell or a position on the solid surface.

In the case of bounce back boundary conditions a very crude *LEGO* approximation is only possible. Due to the chosen positions of the circle center (x_{center} is integer, i.e. on a lattice line whereas y_{center} is between two lattice lines) the resulting representation is not symmetric in the case of bounce back. For boundary fitting, the surface is smooth and symmetric. Even for low resolutions (i.e. few voxels per diameter), the circle is very well approximated.

It can be expected that in particular for low resolutions or high Reynolds numbers a large difference between the two boundary conditions can be observed. At low resolutions, the *LEGO* effect of the surface representation can be strong. At increasing Re it is also becoming more dominant as the viscous length of the flow is decreasing and thus the flow "feels" smaller and smaller steps which are hidden at lower Reynolds number.

Getting some feeling for the importance of an enhanced representation of the geometric shape is a main motivation for this thesis. For all investigations the code *ANB* is used. This code represents a simple and well documented 2D lattice Boltzmann flow solver for incompressible flows. It is available in different flavors. In the following *ANB* denotes the standard version which uses the bounce back boundary conditions. *ANB_Interpol* denotes the version with boundary fitting boundary conditions of Bouzidi. When using $q = \frac{1}{2}$ for all intersections, *ANB_Interpol*'s operation is identical to the standard *ANB* version.

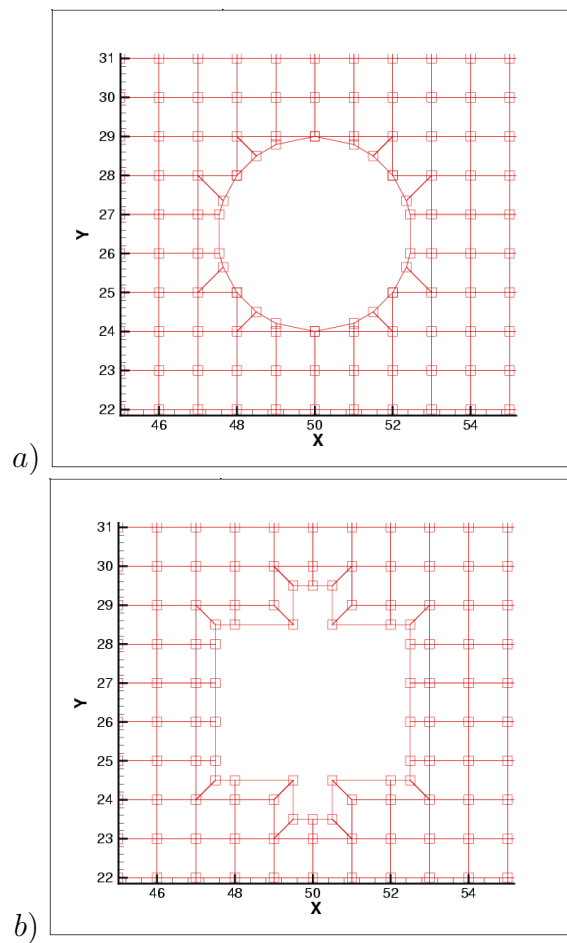


Figure 10: Graphical presentation of the cylinder with a) $ANB_Interpol$ and b) ANB

5 Results and Discussions

The results, explanations and discussions to the tests are presented in this chapter. First the two program codes are juxtaposed and afterwards all investigated cases are evaluated and compared to other experimental and numerical data found in different literature sources.

5.1 Comparison of the Program Codes

Within this bachelor's thesis there was the flow past a circular cylinder chosen for the validation of the program codes, since a number of experiments and theoretical computations concerning this problem can be found in the literature, which can be used as basis for a comparison with the present results. The purpose is to investigate and evaluate the problem of the boundary conditions by the flow past the cylinder in a channel.

β	d	L	H	Re_{mean}	$St(ANB)$	$St(ANB_interpol)$
0.2	20	400	100	62.5	0.2496	0.2501
0.2	20	400	100	69.7	0.2545	0.2571
0.2	20	400	100	83.3	0.2614	0.2686
0.2	20	400	100	97.2	0.2692	0.2784
0.2	20	400	100	118.7	0.2716	0.2876
0.2	20	400	100	131.9	0.2799	0.2939
0.2	20	400	100	145.7	0.2876	0.2968

Table 1: Determination of the Strouhal number for 2 series of calculations for blockage ratios 0.2: comparison of the boundary fitting (*ANB_Interpol*) and the bounce back (*ANB*) models.

A series of test cases for $\beta = 0.2$ in the range $62.5 < Re_{mean} < 145.7$ was carried out and the results for the Strouhal number can be seen in table 1 and the graphical interpretation of the results in figure 11. The comparison of both programs confirmed, that for low Reynolds numbers the resolution in the geometry of the obstacle doesn't play an important role for the evolution of the flow behind it. Yet, its importance grows with growing Re till a constant difference of about 0.0120 between the St values is attained for this range of Reynolds numbers. In figure 12 one can see how different the run of the vertical velocity component is for the two geometrical forms at higher Re . By the *LEGO*-model the break-off point is more precisely defined, that's why the oscillations are stronger. Otherwise *ANB_Interpol* simulates smooth surface and the break-off point displaces.

ANB_Interpol's even surface is also the reason why the streamlines around the cylinder run closer to its boundary compared to those in the case when the *LEGO*-model is implemented, which are more out-lying. By the exact circular form the stream can smoothly

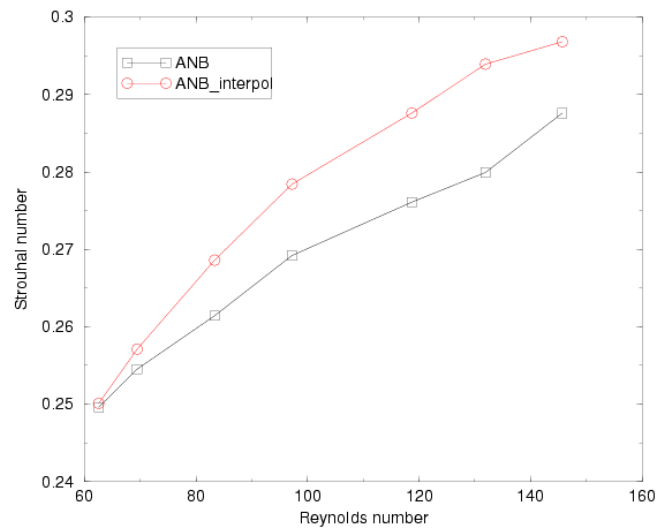


Figure 11: Reynolds-Strouhal number relation for *ANB* and *ANB_Interpol*

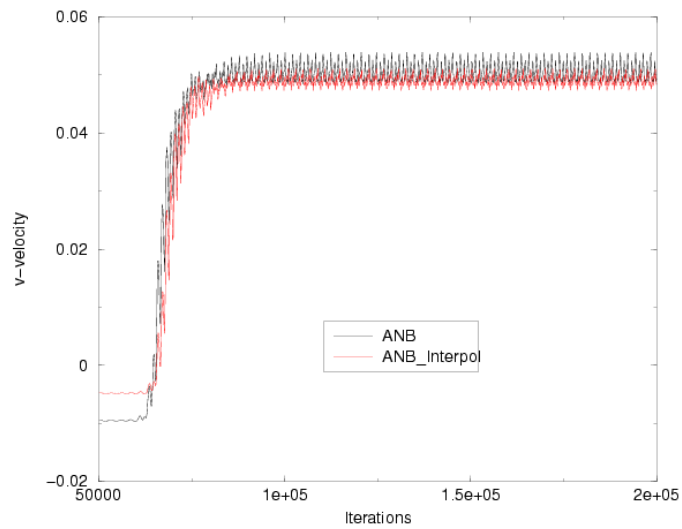


Figure 12: The time development of the *v*-velocity computed with *ANB* and *ANB_Interpol* in point with coordinates $x = \frac{L}{2}$ and $y = \frac{H}{2} + 0.5$ in a Cartesian coordinate system starting in the low left corner of the computational domain. $Re_{mean} = 131.9$ and $\beta = 0.2$.

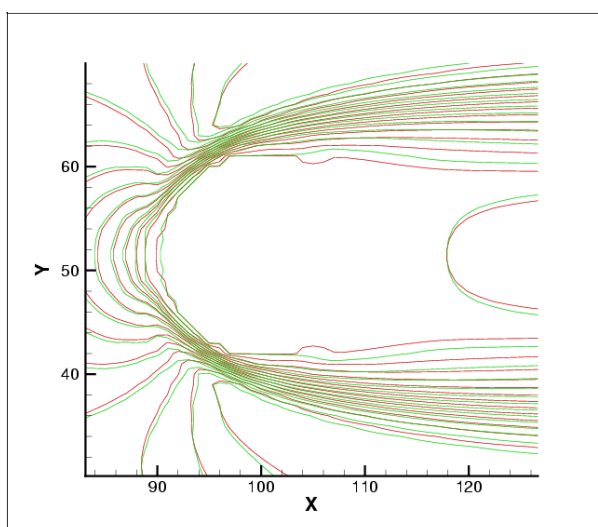


Figure 13: Isoplots of the stationary development of the u -velocity for *ANB_Interpol* in red and *ANB* in green

slip over the surface and the streamlines remain close to the body. Unlike this model, when the *LEGO* geometry is displayed, this easy slipping is impeded and the stream is reflected and repelled further from the cylinder, as shown in figure 13.

In the present work, tending to present an evaluation of improved boundary conditions by means of the boundary-fitting model described above, all further numerical simulations are performed with *ANB_Interpol*.

5.2 Influence of the Domain Length

In order to verify to which extend the length of the computational domain affects the results of the numerical simulations a series of calculations at different channel lengths was carried out (see table 2) and the length-to-diameter ratio was plotted against the Strouhal number (figure 14). The blockage ratio in all cases was constant $\beta = 0.1$, the channel height and the diameter of the cylinder as well ($H = 100$ and $d = 10$), and only the x-axis of the computational domain varied between 200 and 1600 units. As the plot shows, the value of the Strouhal number in the case where the horizontal span of the channel is only twice longer as its width is notably higher than all other values, which makes us arrive at the conclusion, that a minimum length is necessary, so that no disturbances caused by the inflow and outflow occur. In the other three cases the value of the Strouhal number rises slightly by increasing the length-to-diameter ratio.

For the purpose of making the difference among the factors by which the Strouhal number changes from case to case more distinguishable we can convert those differences in percent. From this conversion can be seen, that the Strouhal number in the second case ($L : d = 40$) is around 2.69% smaller than the one in the first case ($L : d = 20$); the one in the third case ($L : d = 80$) is only 0.59% higher than that in the second case and St from the

d	L	H	f	U_{mean}	Re_{mean}	St
10	200	100	0.0813	0.0347	69.5	0.2336
10	400	100	0.0791	0.0347	69.5	0.2280
10	800	100	0.0796	0.0347	69.5	0.2294
10	1600	100	0.0800	0.0347	69.5	0.2305

Table 2: Variation of the domain length: estimation of the Strouhal number for $\beta = 0.1$ and different length-to-diameter ratios. Horizontally the center of the cylinder is placed at $\frac{L}{4}$ from the inlet of the channel

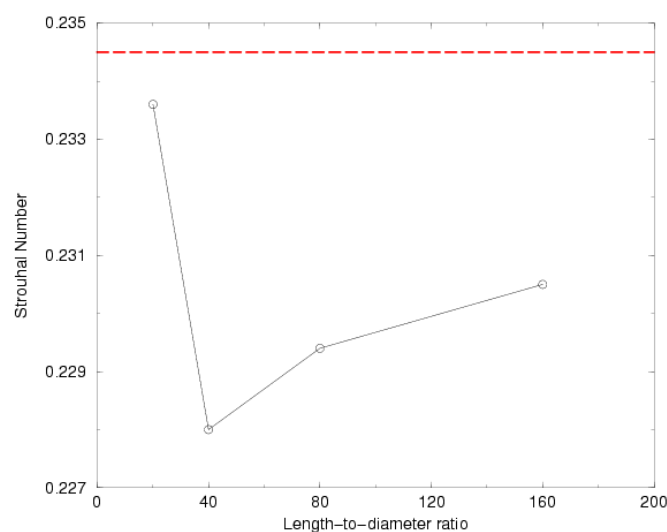


Figure 14: Relation between the length-to-diameter ratio and the correspondent Strouhal number

last calculation ($L : d = 160$) is also only 0.52% higher compared to the previous case. The last three values can be regarded as belonging to the same range and we can draw a conclusion, that at least a length-to-diameter ratio of 40 is required - which is also taken into account in the framework of this thesis.

By applying Richardson extrapolation as described in [9] the exact solution of the end value of the Strouhal number on grid 160 was calculated. It differs from the value that we have already obtained by the discretization error ϵ_h^d in such a manner:

$$\Phi = \phi_h + \epsilon_h^d \quad (20)$$

where Φ stands for the exact solution, the subscript h is the grid reference spacing and ϕ_h is respectively the Strouhal number obtained for the length-to-diameter ratio of 160. By the estimation of the discretization error first one needs to determine the order of the scheme:

$$p = \frac{\log\left(\frac{\phi_{2h} - \phi_{4h}}{\phi_h - \phi_{2h}}\right)}{\log 2} = \frac{\log\left(\frac{0.2294 - 0.2280}{0.2305 - 0.2294}\right)}{\log 2} = 0.3479 \quad (21)$$

In our case $2h$ stands for the Strouhal value at $\frac{L}{d} = 80$ and $4h$ at $\frac{L}{d} = 40$. Further, the exponent p is inserted in the formula for the discretization error on this grid, which can be approximated by:

$$\epsilon_h^d = \frac{\phi_h - \phi_{2h}}{2^p - 1} = \frac{0.2305 - 0.2294}{2^{0.3479} - 1} = 0.004 \quad (22)$$

Now setting the lateral value in equation 20 will lead us to the exact Strouhal number $St = 0.2345$, which is also plotted as a dashed line on figure 14.

A study devoted to the importance of the length-to-diameter ratio was also carried out by Nishioka and Sato [24]. They ascertained, that the critical Reynolds number for vortex shedding from the cylinder depends strongly on this ratio. If the ratio is large enough vortex shedding takes place at lower Re . As the ratio increases the critical Reynolds number increases as well. Their measurements indicated, that the vortex street behind the cylinder has a spanwise wavelength of 15–20 diameters, which suggests that the vortex shedding does not occur two-dimensionally at large length-to-diameter ratios. As the ratio decreases the standing vortex behind the cylinder is stabilized and vortex shedding does not take place until larger Reynolds numbers.

5.3 Influence of the Obstacle Size

Another series of computations (table 3) was accomplished which aims to give a clear answer of the question for which diameters of the obstacle, considering the resolution of the domain, simulations are reasonable. The diagram in figure 15 shows, that in the interval $d = 10$ up to $d = 40$ the values of the Strouhal number differ less than 1% from each other. Only the value for Strouhal number at $d = 5$ is 14% smaller than the one of the subsequent diameter.

The same calculations were done for the case without improved boundary conditions, i.e. with the standard bounce-back model. Right here, in the study of the resolution dependence the *LEGO* effect is explicitly apparent. For the low diameter values the difference in the Strouhal numbers obtained with both program codes is distinguishable. By the time we get to $d = 20$ the difference is minimal and for $d = 30$ both programs deliver the same result for the Strouhal number.

On the basis of the computations described above an obstacle diameter of 20 units was preferred for all further simulation cases within the scope of this work.

d	L	H	f	Re_{mean}	$St(ANB_Interpol)$	$St(ANB)$
5	200	50	0.1390	68.6	0.1915	0.1897
10	400	100	0.0792	68.6	0.2282	0.2242
14	560	140	0.0569	68.6	0.2322	0.2290
20	800	200	0.0400	68.6	0.2360	0.2353
30	1200	300	0.0267	68.6	0.2377	0.2377
40	1600	400	0.0200	68.6	0.2381	-
50	2000	500	0.0160	68.6	0.2381	-

Table 3: Variation of the resolution: results of the Strouhal number at blockage ratio 0.1 and different size of the obstacle and the channel

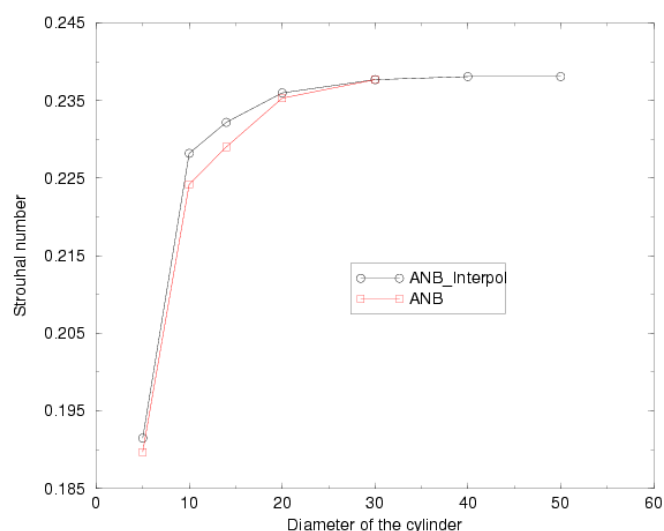


Figure 15: Strouhal number for different diameters of the cylinder

5.4 Influence of the Blockage Ratio

Simulations for three different blockage ratios were carried out: 0.1, 0.2 and 0.4 and due to the outcomes systemized in table 4 and graphically interpreted in figure 16 can be deduced, that by increasing the blockage ratio the Strouhal number also shifts upwards to higher values.

A similar phenomenon was observed by Zovatto and Pedrizzetti [38] as they analyzed the transition from steady flow to a periodic vortex shedding regime by placing the cylinder closer to one of the channel walls. The researchers claimed, that neither the velocity profile nor the local irrotational acceleration which occurs only on one side of the body and is reduced on the opposite side can explain the delay in the transition. The reason is, that as the body approaches the wall a local acceleration and deceleration occurs on the wall itself, this produces higher vorticity values in the wall boundary layer and rapidly grows downstream and influences the cylinder wake. The cylinder wake is stabilized by coupling with the wall vorticity, and so it does not oscillate in a shedding regime.

β	d	L	H	f	U_{mean}	Re_{mean}	$St(ANB)$
0.1	20	800	200	0.0400	0.0347	69.7	0.2360
0.2	20	400	100	0.0446	0.0347	69.7	0.2571
0.4	20	200	50	0.0600	0.0347	69.7	0.33371
0.1	20	800	200	0.0429	0.0350	83.7	0.2524
0.2	20	400	100	0.0466	0.0350	83.7	0.2686
0.4	20	200	50	0.0748	0.0350	83.7	0.4121

Table 4: Variation of the blockage ratio: Strouhal number dependent on the blockage ratio

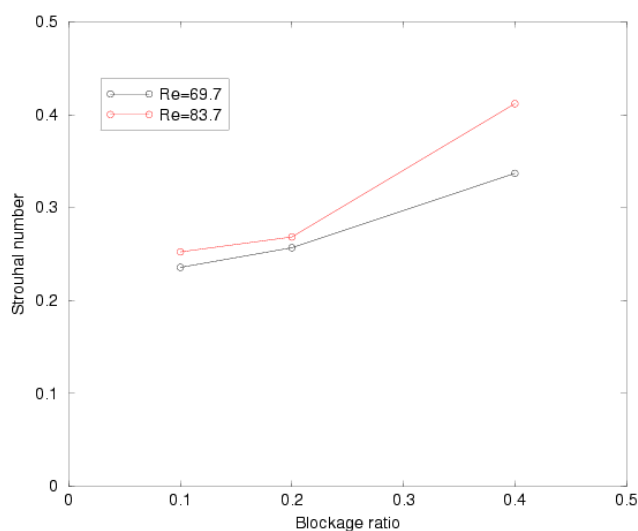


Figure 16: Results for Strouhal number as a function of the blockage ratio

This assumption is confirmed by the numeric investigation of Chen et al. [6]. In their study the Strouhal numbers for different blockage ratios and different critical Reynolds numbers based on the cylinder diameter are numerically estimated and the graphical interpretation of the results are shown in figure 17 .

The increment of the diameter-to-width ratio evokes another effect of postponement of the critical Reynolds number, which can also be seen by the present calculations in figure 19. By the accomplishment of the numerical simulations for the series of Reynolds numbers it is eye-catching, that the periodic detachment for blockage ratio 0.1 starts before the oscillations for $\beta = 0.2$. A few more numerical and experimental studies confirm the correction of this observation. The subject can be found in the numerical simulations by Chen et al. [7], as well as in the experimental works by Coutanceau and Bouard [8] and Shair [27].

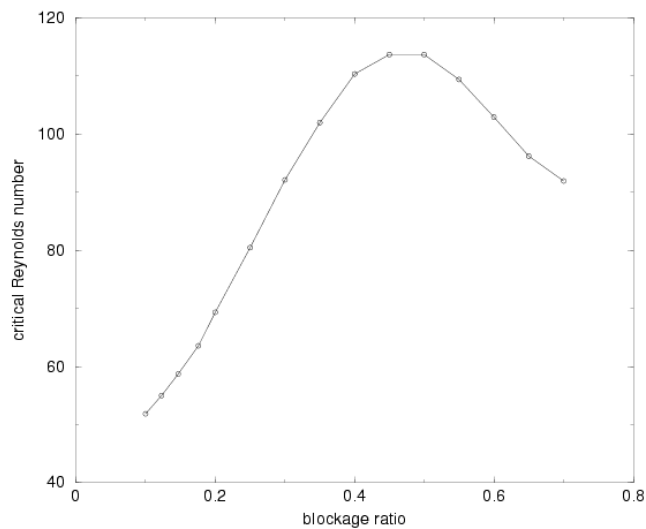


Figure 17: Chen et al.'s [6] results for the relation between the blockage ratio and the critical Reynolds number based on the cylinder diameter, as described in section 2.1.

5.5 Simulations at Reynolds = 131.9

In figure 7a a cut of the time-development of the v -velocity in point with coordinates $x = \frac{L}{4}$ from the length and $y \approx \frac{H}{2}$ at $Re_{mean} = 131.9$ and $\beta = 0.2$ is presented. The time development of the v -velocity itself can be seen in figure 12: the first periodic fluctuations are in sight after 65000 iterations and after 85000 iterations they attain a constant amplitude.

A closeup look of the course of the streamlines in the obstacle's surrounding can be seen in figure 18. The eddies circulating behind the cylinder begin to oscillate and break off from the cylinder. They are dragged downstream as discrete *parcels* of vorticity and frame the vortex street. How are the vortices produced? The explanation offered in [10] is the following: the fluid velocity at the surface of the cylinder must be zero and increases rapidly away from that surface. When the main stream velocity is low enough, there is sufficient time for this vorticity to diffuse out of the thin region near the solid surface where it is produced and to grow into a large region of vorticity.

5.6 Former Investigation of Circular Cylinder

Among the numerous experimental and numerical studies concerning the problem of a circular cylinder emerged in a free-stream only those will be mentioned, which contain information about the development of the Reynolds-Strouhal number relation. Moreover, in all but one works, that were found, the flow is considered unbounded, which doesn't help us much by the validation of the data for the different blockage ratio cases. That

caused a restriction of the number of former investigations, which results are included in the present work.

5.6.1 Yokoi's Experimental Work

Yokoi [36] performed a number of experiments in order to investigate the vortex shedding of a circular cylinder in a rectangular duct. His experimental apparatus for the parallel wall case included a test section with cross sectional area size $60\text{mm} \times 70\text{mm}$ and a mounted brass cylinder with diameter 5mm and span length 60mm , hence the ratio between the height of the duct and the diameter of the cylinder (blockage ratio) of around 0.07. The investigated Reynolds numbers were in the range between $Re = 100 \sim 5000$, but because of the much more restricted scope to which the Reynolds numbers of the present thesis belong only the few values of Yokoi up to $Re = 250$ are inset as basis for comparison. Much more interesting is the conclusion of his experimental study, confirmed by a few numerical experiments of his: he deduced, that as the Reynolds number increases, the Strouhal number tends to increase as well, at least up to $Re = 1000$. Over Reynolds of 1000 the values of Strouhal number are held constant the same as Strouhal in the case of unbounded domain.

5.6.2 The Investigations of Williamson

Williamson [31], [32], [33] is one of researcher who over a few years engaged in the investigation of the Strouhal-Reynolds number relation and the phenomenon of oblique and parallel modes of vortex shedding. In his experimental study from 1988 [31] he explained why a considerable difference in the vortex shedding frequency appears, which is namely due to a change in the mode of oblique shedding. By manipulating the end conditions and this way inducting parallel shedding he achieved a completely continuous Strouhal curve which agrees with the oblique shedding by a $\cos \theta$ relation, where θ is the oblique-shedding angle. For a comparison with numeric results he introduced the formula

$$St = \frac{-3.3265}{Re} + 0.1816 + 0.00016 \cdot Re \quad (23)$$

which closely gives the $St - Re$ relation.

In his later work from 1992 [33] he observed the existence of two models of formation of streamwise vorticity in the near wake. The first mode occurs beyond $Re > 180$ and is characterized by regular streamwise vortices appearing in the wake with a wavelength of approximately three cylinder diameters. The second, beyond $Re > 230$, corresponds to the appearance of more irregular array of streamwise vortices with a mean spanwise wavelength of about one cylinder diameter. Between 230 and 260 the first model dominates, whereas at $Re \approx 260$ the second model structures contain more energy - in this range both models coexist.

Only the results for the Strouhal number from Williamson’s experimental study [31] are included in the present research project. The measurements have been made with a cylinder with diameter $d = 0.104$ in the circular section of an openjet wind tunnel with $L/d = 90$.

5.6.3 Karniadakis and Triantafyllou’s Numerical Study

In their study from 1989 Karniadakis and Triantafyllou [20] tried to identify the asymptotic states that can develop in laminar wakes. The approach was that of a direct numerical simulation using the spectral-element method and a high-order, weighted residual technique, which combines the accuracy of spectral methods with the flexibility in geometry of finite-element schemes. In the spectral-element mesh used in the calculations very high resolution was placed around the cylinder in order to accurately compute the boundary layer. The cylinder geometry was represented exactly, as isoparametric expansions were employed to map the curvilinear elements onto standard squares. The boundary conditions on the computational mesh were taken to be uniform oncoming flow, potential flow at the side “walls”, no-slip on the cylinder surface and outflow Neumann conditions at the downstream boundary. The result for Reynolds number equal to 100 was compared to Roshko’s [26] empirical formula and it turned out that, the value of Strouhal number predicted by Karniadakis and Triantafyllou was about 8% higher than the experimental one. In order to investigate the discrepancy, they tested the accuracy of the calculations by using a mesh with much higher resolution and it yielded the same results. Afterwards they repeated the calculation once again with different mesh, twice as wide as the the first one - the Strouhal number was reduced by 2%. So they concluded, that the disagreement between their computations and Roshko’s experiments can be partly attributed to the truncation of the computational domain, or errors might also be caused in the experimental measurements, introduced by the three-dimensionality of the flow.

5.6.4 The Numerical Research of Thompson et al.

Thompson, Hourigan and Sheridan [30] undertook numerical experiment for the purpose of computing the two- and three-dimensional wake structure behind a circular cylinder and compared their predictions for the two-dimensional case with other experimental results. Their governing equations were the incompressible time-dependent Navier-Stokes equations in primitive variable form and were discretized using a time-split spectral/spectral element method as described by Karniadakis and Triantafyllou [21]. The spectral element mesh consisted of 106 macroelements. Each element was mapped into a computational square, and high-order Lagrangian polynomial interpolants were used to approximate the solution variables in each directions. The inflow and outflow boundary conditions were taken from potential flow solution. Also, the outflow boundary conditions were taken to be $\frac{\partial v}{\partial n} = 0$ and $p = 0$. The domain presented a two-dimensional semi-circle which stretched in front of the cylinder to its poles. The radius of the semi-circle is varied up to $X_i = 50R$, where R is the radius of the cylinder. Behind the obstacle the mesh is elongated in a

rectangular form with length up $X_0 = 42.6R$. Calculations were done for different size of the mesh and also compared to Williamson's experimental data [31]. The results for the large domain were within 1% of the experimental values.

5.6.5 Persillon and Braza's Numerical Simulation

H. Persillon and M. Braza also concentrated their attention to the problem of analyzing the transition to turbulence in a wake of a cylinder. In their article published in 1998 [25] this is studied by a numerical simulation based on the three-dimensional full Navier-Stokes equation for a compressible fluid in the Reynolds number range 100-300. The numerical method is second order accurate in space and time and Neumann boundary conditions are used at the two boundaries in spanwise direction; $u = 1$, $v = 0$ and $w = 0$ at the inlet and non-reflecting (absorption) boundary conditions are specified for the outlet downstream boundary. In the physical domain the flow was not confined; nevertheless, fictitious external boundaries were set far from the cylinder. Also in the spanwise z -direction the cylinder is supposed to be infinite. A striking difference in the Strouhal number between the two- and three-dimensional cases was ascertained: for each Reynolds number the three-dimensional Strouhal number is lower than the two-dimensional one, which is in a very good agreement with the experiments of Williamson (1998) [31], who has shown discontinuities in the St-Re-relation.

5.6.6 Zovatto and Pedrizzetti's Study of Cylinder Between Parallel Walls

In 2001 Zovatto and Pedrizzetti released an article [38] which topic is the laminar flow inside a channel in the presence of circular cylinder. The channel is plane with rectilinear walls separated by a distance h , the diameter of the cylinder is d and its positions are defined by the gap Δ , the minimal distance from the cylinder surface to the nearest wall. The fluid is considered incompressible, following the steady average velocity U_{mean} inside the channel. The problem is made dimensionless by taking h as the unit length, $\frac{h}{U_{mean}}$ as the unit time and ρh^3 as the unit mass. The problem is governed by three dimensionless parameters: the channel Reynolds number $Re_{channel} = \frac{U_{mean}h}{\nu}$, the blockage ratio β and the gap parameter $\gamma = \frac{\Delta}{d}$. In order to be able to compare Zovatto and Pedrizzetti's results with those from the present study we are interested only in the case, where the cylinder is placed in the middle of the channel, which means that the gap parameter will take its maximal value $\gamma = 2$ for the fixed value of the blockage ratio $\beta = 0.2$ used in that study. Later on they introduced another cylinder-based Reynolds number

$$Re_{cyl} = ReU_{cyl}\beta \quad (24)$$

where U_{cyl} is the average velocity in front of the cylinder far upstream and

$$U_{cyl}(\gamma) = -6\beta^2\gamma^2 + 6\beta(1 - \beta)\gamma + \beta(3 - 2\beta) = 1,48 \approx \frac{3}{2} \quad (25)$$

When one inserts this value in formula 24 this would mean that the velocity is multiplied by factor $\frac{3}{2}$ and this is nothing but the free-stream velocity U_∞ . And we know that we have to multiply the free-stream velocity with $\frac{2}{3}$ in order to obtain the mean velocity U_{mean} . This way the terms $\frac{3}{2}$ and $\frac{2}{3}$ cancel, we only have to multiply $Re_{channel}$ with the blockage ratio 0.2 and it yields the Reynolds number on terms of the mean velocity in the channel.

The authors reported a table where the dimensionless period T was presented as a function of the channel Reynolds number and the gap parameter. By means of equation 24 and the mathematical operations described above we can easily convert the released values of Reynolds to Re_{mean} . On the other hand they defined the Strouhal number as

$$St = \frac{\beta}{U_{cyl}T} \quad (26)$$

so we are provided with all the data in order to calculate the Strouhal numbers and thus setting the $St - Re_{cyl}$ relation. The last point we should take into account is that in the expression for the Strouhal number the velocity should be multiplied by $\frac{2}{3}$ in order to set in the average velocity. After all this a Strouhal number range between $St \approx 0.23$ and $St \approx 0.3$ is obtained, which is in best accordance with the results from the present work.

5.6.7 Juxtaposition of the Results

The parameters and outputs of the cases investigated within the scope of this bachelor's thesis are reported in table 5. Because of the restricted number of studies handling with channel confined by walls, we concentrated on the computations with relatively small blockage ratios — 0.1 and 0.2, where the distance between the cylinder and the wall is as large as possible and thus the investigated cases are relatively close to the simulations or experiments with unbounded flows, which should help us by the validation of the obtained data.

In the graphical evaluation of the data in figure 19 one can clearly see, that although the results from the different studies deliver so different values for the Strouhal number, they all have something in common — the run of the curves representing the the $St - Re$ relation. In this sense the curves obtained in the present thesis can be considered as a parallel displacement of some of the other curves to a higher Strouhal number scope. And the reason for this displacement can be found in the specification of the boundary conditions of the domain. While in all other studies, apart from the one by Zovatto and Pedrizzetti, the domain is unbounded, the present work is characterized by the introduction of channel walls, which evoke the establishment of a parabolic velocity profile and thus exert influence on the u -velocity value by the calculation of the Strouhal number. The Strouhal numbers obtained on the basis of the data reported by Zovatto and Pedrizzetti belong to exactly the same range as the present results.

Similar investigations dealing with the vortex shedding behind a square obstacle [37] showed, that dependence of the blockage ratio exists - with increasing diameter-to-height

β	d	L	H	f	U_{mean}	Re_{mean}	St
0.1	20	800	200	0.0429	0.0340	54.4	0.2206
0.1	20	800	200	0.0400	0.0340	68.0	0.2353
0.1	20	800	200	0.0429	0.0340	81.6	0.2524
0.1	20	800	200	0.0430	0.0340	95.2	0.2547
0.1	20	800	200	0.0450	0.0340	112.2	0.2646
0.1	20	800	200	0.0469	0.0340	125.8	0.2756
0.1	20	800	200	0.04832	0.0340	142.8	0.2842
0.2	20	400	100	0.0434	0.0347	62.5	0.2501
0.2	20	400	100	0.0446	0.0347	69.7	0.2571
0.2	20	400	100	0.0466	0.0347	83.3	0.2686
0.2	20	400	100	0.0483	0.0347	97.2	0.2784
0.2	20	400	100	0.0499	0.0347	118.7	0.2876
0.2	20	400	100	0.0510	0.0347	131.9	0.939
0.2	20	400	100	0.0515	0.0347	145.7	0.2968

Table 5: Table of the test cases - estimation of the Strouhal number for 2 series of calculations for blockage ratios 0.1 and 0.2

ratio higher Strouhal numbers are set. We don't have the necessary database at our disposal for such comparison in the case of a circular cylinder, but we drew the same conclusion in our study in section 5.4 and this can be also seen in figure 19.

Regarding the magnitude of Strouhal number, basically there are no considerable differences among the included publications, the only small exception is Yokoi's experimental data. By the introduction of Persillon and Braza's results it was mentioned, that they observed significant distinction between the two- and three-dimensional case and that the 3D simulations yielded lower Strouhal numbers. This could explain why Yokoi's values, fruit of a three-dimensional experiment lie under the numerical curves. Moreover, only few values from Yokoi belong to our restricted Re range and the probability of wrong inferences because of insufficient information is very high.

Since in the referred studies the information about the evaluation methods and the convergence behavior in the numeric computations is not comprehensive, it's hard to determine their accuracy and their authenticity.

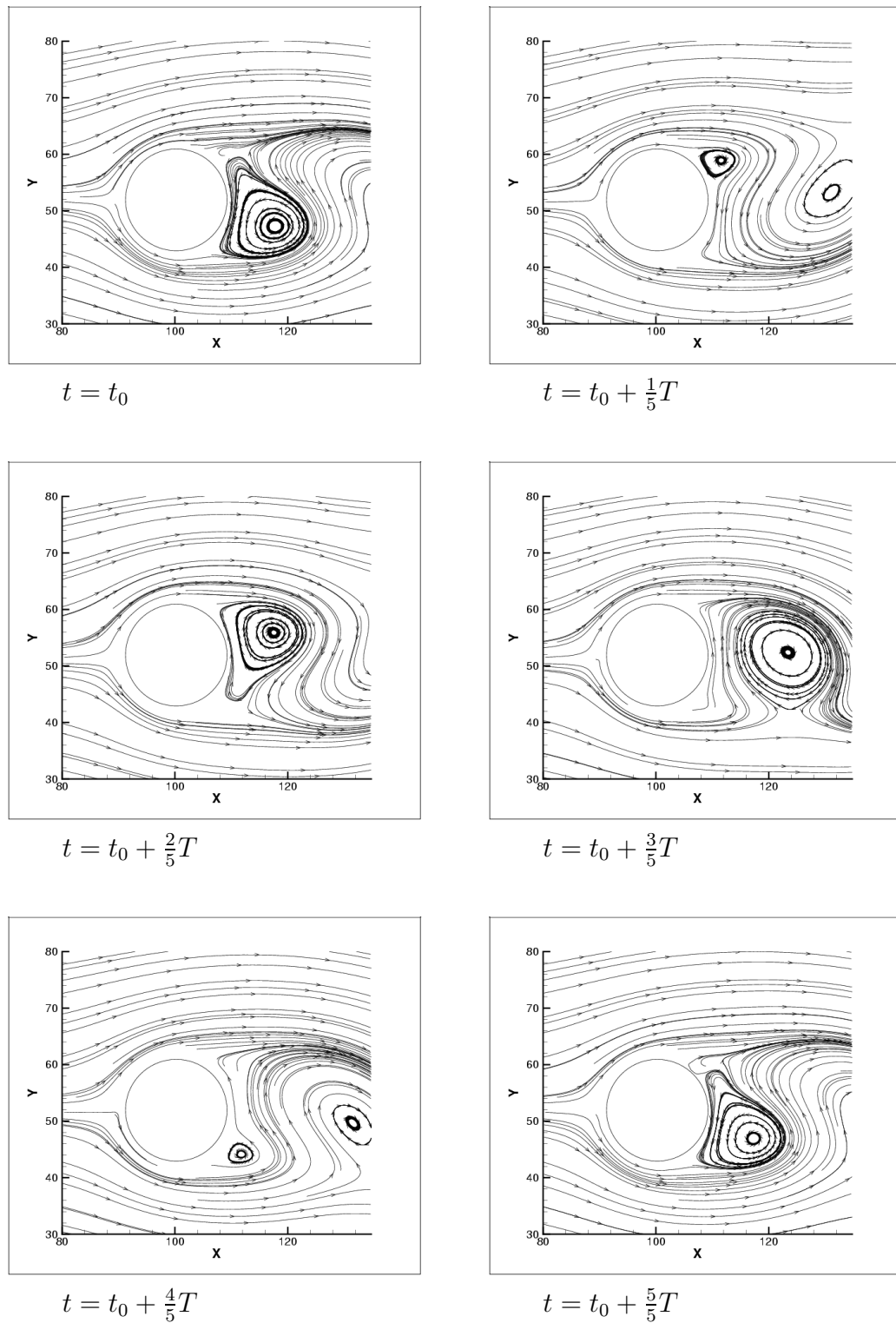


Figure 18: Streamline plot of the flow close to the cylinder presenting one period in the vortex appearance, development and detachment at $Re_{mean} = 131.9$

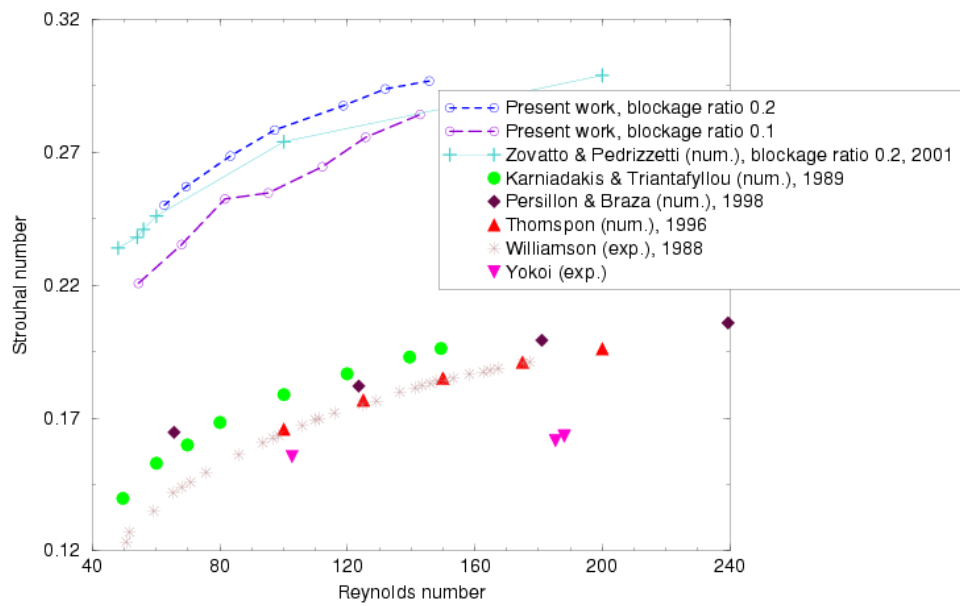


Figure 19: Graphical presentation of former studies compared with the results for Strouhal number from the present work. Both Reynolds number and Strouhal number are function of the mean inflow velocity U_{mean} which is approximately $\frac{2}{3}$ of the specified velocity U_{max} .

6 Summary

In this bachelor's thesis, the problem of the boundary conditions in the case of flow past a circular cylinder in a channel was examined. For this purpose an alternative concept introducing the boundary-fitting mechanism in the presence of boundaries and an exact circular form were implemented in the program code *ANB_Interpol* and evaluated on the basis of comparisons with the results from former investigations of the same flow-obstacle configuration.

The work starts with two chapters that draw one's attention to the theory behind the problem of a flow past a circular cylinder, the physical and numerical background. First the relevant dimensionless numbers, the flow regimes behind a circular obstacle, the influence of the channel walls and the computational domain on the flow were discussed. After that the lattice Boltzmann approach was introduced in the next chapter.

The next step was to collate the program code with its predecessor, the algorithm of depiction of the circular form with *ANB_Interpol* was briefly presented, accompanied by illustration of the geometric models. The reasons for the different results that both codes yielded were described and explained — by means of the two different geometric presentations and boundary condition approaches that both programs suggest, conclusions were drawn and predictions can be made about the development of the vortex street behind the cylinder. Different run of the streamlines around the obstacles was observed and explained, as well as the results for the Strouhal number computed with both program codes were systemized.

Further simulations were carried out with *ANB_Interpol* and the influence of different parameters on the establishment and evolution of vortex shedding were evaluated and compared with other studies.

The first investigated parameter was the length of the channel included in the diameter-to-length ratio, which investigation showed, that there is a minimal ratio which should be selected by the simulations in order to obtain reasonable results. This ratio is of interest also for the critical Reynolds number: the larger the diameter-to-length ratio is, the sooner the periodic detachments behind the cylinder start.

The size of the cylinder was the next subject of investigations. For it the same deduction is valid - considering the resolution of the domain a minimal diameter of the circle $d = 10$ is required, thereby one should take into account, that the differences between the Strouhal numbers obtained by the use of the two program codes depend on the resolution — the worse the resolution is, i.e. the smaller the diameter of the cylinder is, the more obvious this difference is.

Finally, the importance of the blockage ratio by the different test cases was discussed. Although in none of the former works dealing with circular cylinder this ratio was studied, the results from the present study could be validated by referring to data achieved by the evaluation of a flow past square obstacle [37]. The present computations once again

confirmed, that by raising the blockage ratio the critical Reynolds number the values of the Strouhal number rise too.

Despite the simple configuration of the problem and despite the numerous works on the topic, the results that can be found are not sufficient. In this sense future experimental and numerical investigations of the flow past circular cylinder can be performed, especially in the case when channel walls confine the domain.

Appendix

List of Figures

1	A two-dimensional presentation of the drag and lift coefficient acting on the cylinder	5
2	Profile of the free-stream velocity when there are no confining walls	6
3	Profile of the velocity with confining walls	6
4	Scheme of the channel	20
5	Development of the v -velocity in the point with coordinates $x = \frac{L}{2}$ and $y = \frac{H}{2} + 0.5$ in a coordinate system based on a cartesian coordinate system starting in the low left corner of the computational domain. $Re_{mean} = 131.9$, $\beta = 0.2$	22
6	A closeup look at a) the v -velocity and b) and c) the power density spectrum plotted against the Strouhal number for $\beta = 0.2$ and $Re_{mean} = 83.3$. In b) the marked cell from which the evolution of v -velocity was observed was placed vertically about $\frac{H}{10}$ from the middle of the channel and in c) the distance is about $\frac{H}{5}$. Although in the power density spectrum three separate peaks of different height can be recognized, the value for St is always yielded from the first one	23
7	A closeup look at a) the v -velocity and b) the power density spectrum plotted against the Strouhal number for $\beta = 0.2$ and $Re_{mean} = 131.9$. The cell from which the v -velocity was measured lied in about the middle of the channel, that's the reason why the first peak is not the highest in this presentation. The coexistence of more peaks is due to the fact, that additional detachment modes at high Reynolds numbers cause additional disturbances. Again the Strouhal number is read off from the very first peak.	24
8	The boundary-fitting model applied by the collision of the particles at a wall	26
9	Octagonal lattice cell	26
10	Graphical presentation of the cylinder with a) $ANB_Interpol$ and b) ANB	28
11	Reynolds-Strouhal number relation for ANB and $ANB_Interpol$	30
12	The time development of the v -velocity computed with ANB and $ANB_Interpol$ in point with coordinates $x = \frac{L}{2}$ and $y = \frac{H}{2} + 0.5$ in a Cartesian coordinate system starting in the low left corner of the computational domain. $Re_{mean} = 131.9$ and $\beta = 0.2$	30
13	Isoplots of the stationary development of the u -velocity for $ANB_Interpol$ in red and ANB in green	31

14	Relation between the length-to-diameter ratio and the correspondent Strouhal number	32
15	Strouhal number for different diameters of the cylinder	34
16	Results for Strouhal number as a function of the blockage ratio	35
17	Chen et al.'s results for the relation between the blockage ratio and the critical Reynolds number based on the cylinder diameter, as described in section 2.1.	36
18	Streamline plot of the flow close to the cylinder presenting one period in the vortex appearance, development and detachment at $Re_{mean} = 131.9$. .	42
19	Graphical presentation of former studies compared with the results for Strouhal number from the present work. Both Reynolds number and Strouhal number are function of the mean inflow velocity U_{mean} which is approximately $\frac{2}{3}$ of the specified velocity U_{max}	43

List of Tables

1	Determination of the Strouhal number for 2 series of calculations for blockage ratios 0.2: comparison of the boundary fitting (<i>ANB_Interpol</i>) and the bounce back (<i>ANB</i>) models.	29
2	Variation of the domain length: estimation of the Strouhal number for $\beta = 0.1$ and different length-to-diameter ratios. Horizontally the center of the cylinder is placed at $\frac{L}{4}$ from the inlet of the channel	32
3	Variation of the resolution: results of the Strouhal number at blockage ratio 0.1 and different size of the obstacle and the channel	34
4	Variation of the blockage ratio: Strouhal number dependent on the blockage ratio	35
5	Table of the test cases - estimation of the Strouhal number for 2 series of calculations for blockage ratios 0.1 and 0.2	41

Index of Symbols

c	speed of sound
\vec{c}_i	particle velocity vector in i -direction
C_D	drag coefficient
C_L	lift coefficient
d	characteristic length; diameter of the cylinder
\vec{e}_i	discrete velocity; \vec{e}_{i_α} ; \vec{e}_{i_α} lattice vectors
f	particle distribution function
f	detachment frequency
f_{max}	maximum frequency
f_s	sampling rate
F	body force per unit mass
$F_{D\nu}$	viscosity force of the drag coefficient
F_{Dp}	pressure force of the drag coefficient
$F_{L\nu}$	viscosity force of the lift coefficient
F_{Lp}	pressure force of the lift coefficient
h	reference spacing of the grid
H	channel height
$i = 0 \cdot \cdot N$	index of the local lattice link
l_u	diagonal in the octagonal computational mesh
k	offset between the inclined lines of an octagonal lattice grid
L	channel length
n_x	x -component of the normal vector to the cylinder surface S
n_y	y -component of the normal vector to the cylinder surface S
N_i	distribution function
N_i^{eq}	discretized Maxwell-Boltzmann distribution function
p	order of convergence
p	pressure
q	location of the wall on the computational grid
R	radius of the cylinder
S	cylinder surface
t	current time
t_p	lattice direction dependant constant
t_u	time interval for which a particle moves from one node to another
Δt	period duration
T	dimensionless period
u	axial velocity component
\vec{u}	macroscopic velocity
U_{max}	maximal velocity in front of the parabolic velocity profile
U_{mean}	mean velocity = $\frac{2}{3}U_\infty$
U_t	tangential velocity
U_∞	free-stream velocity
v	radial velocity component
\vec{x}	local node

Greek Letters

β	diameter-to-height ratio; blockage ratio
γ	gap parameter
$\delta_{\alpha\beta}$	Kroneker-Delta operator
Δ	gap, the minimal distance from the cylinder surface to the nearest wall
ϵ_h^d	discretization error
μ	dynamic viscosity
ν	kinematic viscosity
$\vec{\xi}$	particle velocity
ρ	density
ϕ_h	solution of discretized equation on a grid h
Φ	exact solution of a partial differential equation
ω	relaxation parameter
Ω	collision integral

Dimensionless numbers

$Ma = \frac{U}{c}$	Mach number
Re_c	critical Reynolds number ; Reynolds number from which the periodic detachment starts
$Re_{channel} = \frac{U_{mean}h}{\nu}$	channel Reynolds number
$Re_{cyl} = ReU_{cyl}\beta$	cylinder-based Reynolds number
$Re_{mean} = \frac{U_{mean}d}{\nu}$	actual Reynolds number on terms of the mean velocity set in the channel and the size of the obstacle
$Re_{\infty} = \frac{U_{\infty}d}{\nu}$	Reynolds number in terms of the free-stream velocity and the size of the obstacle
$St = \frac{fd}{U_{mean}}$	Strouhal number in the channel in terms of the mean velocity and the characteristic length of the obstacle

References

- [1] A. Acrivos, L. G. Leal, D. D. Snowden, F. Pan:
Further experiments on steady separated flows past bluff objects.
J. Fluid Mech. 34, 1968, pp.25 – 48.
- [2] J. Bernsdorf:
Strömungsbereshnungen mit Lattice-Boltzmann-Automaten.
Kurzlehrgang NUMET, LSTM, Universität Erlangen-Nürnberg, 2000
- [3] M. Bouzidi, M. Firdaouss, P. Lallemand:
Momentum transfer of a Boltzmann-lattice fluid with boundaries.
Phys. Fluids 23 (11), 2001, pp.3452 – 3459.
- [4] J. Buick:
Lattice Boltzmann Methods in Interfacial Wave Modelling.
<http://www.ph.ed.ac.uk/~jmb/thesis/tot.html>
- [5] I. Celik:
Analytical modeling of the mean flow around circular cylinders - A Review.
Symp. on Advancements in Aerodynamics, Fluid Mech. and Hydraulics, Minneapolis,
Minnesota, June 3 – 6, 1986
- [6] J.-H. Chen, W. G. Pritchard, S. J. Tavener:
Bifurcation for flow past cylinder between parallel planes.
J. Fluid Mech. 284, 1995, pp.23 – 41.
- [7] J.-H. Chen:
Laminar separation of flow past a circlar cylinder between two parallel plates.
Proc. Natl. Sci. Coun. ROC(A) 24 (5), 2000, pp.341 – 351.
- [8] M. Coutanceau, R. Bouard:
Experimental determination of the main features of the viscous flow in the wake of a circular cylinder in uniform translation. Part 2. Unsteady flow.
J. Fluid Mech. 79, 1977, pp.257 – 272.
- [9] J. H. Ferziger, M. Perić:
Computational Methods for Fluid Dynamics.
1996, Springer.
- [10] *Flow visualisation: Flow around a cylinder at Reynolds number 40 – 200.*
<http://www.cwr.uwa.edu.au/cwr/teaching/flowvis/flowvis.htm>
- [11] B. Fornberg:
A numerical study of steady viscous flow past a circular cylinder.
J. Fluid Mech. 98 (4), 1980, pp.819 – 855.

-
- [12] R. Franke:
Numerische Berechnung der instationären Wirbelablösung hinter zylindrischen Körpern.
PhD-Thesis, Fakultät für Bauingenieur- und Vermessungswesen, Universität Friederici-
ciana zu Karlsruhe, 1991.
- [13] U. Frisch, B. Hasslacher, Y. Pomeau:
Lattice-gas automata for the Navier-Stokes equation.
Phys. Rev. Lett. 56, 1986, pp.1505 – 1508.
- [14] U. Frisch, D. d’Humières, B. Hasslacher, P. Lallemand, Y. Pomeau, J.-P. Rivert:
Lattice Gas Hydrodynamics in Two and Three Dimensions.
Complex Systems 1, 1987, pp. 649 – 707
- [15] J. R. Graham:
Flow past a cylinder.
<http://astron.berkeley.edu/~jrg/ay202/lectures/node18.html>
- [16] A. S. Grove, F. M. Shair, E. E. Petersen, A. Acrivos:
An experimental investigation of the steady separated flow past a circular cylinder.
J. Fluid Mech. 19, 1965, pp.60 – 80.
- [17] D. Hanon, O. Tribel:
Lattice gas automata.
http://poseidon.ulb.ac.be/simulations/intro_en.html
- [18] J. Hardy, Y. Pomeau, O. de Pazzis:
Time evolution of two-dimensional model system. I. Invariant states and time correlation functions.
J. Math. Phys. 14, 1973, pp.1746 – 1759.
- [19] F. Huber:
Introduction to lattice gas and lattice boltzmann automata in theory and practice.
LSTM - Fereianakademie 2001
- [20] G. M. Karniadakis, G. S. Triantafyllou:
Frequency selection and asymptotic states in laminar wakes.
J. Fluid Mech. 199, 1989, pp.441 – 469.
- [21] G. M. Karniadakis, G. S. Triantafyllou:
Three-dimensional dynamics and transition to turbulence in the wake of bluff objects.
J. Fluid Mech. 238, 1992, pp.1 – 30.
- [22] P. Kiehlm, N. K. Mitra, M. Fiebig:
Numerical investigation of two- and three-dimensional confined wakes behind a circular cylinder in a channel.
AIAA–86 – 0035, 1986.

- [23] Kohno:
Fluid flow simulation by lattice Boltzmann method.
<http://www.fuji-ric.co.jp/prom/complex/kohno/lbmindex.html>
- [24] M. Nishioka, H. Sato:
Measurements of velocity distributions in the wake of a circular cylinder at low Reynolds numbers.
J. Fluid Mech. 65 (1), 1974, pp.97 – 112.
- [25] H. Persillon, M. Braza:
Physical analysis of the transition to turbulence in the wake of a circular cylinder by three-dimensional Navier-Stokes simulation.
J. Fluid Mech. 365, 1998, pp.23 – 88.
- [26] A. Roshko:
On the development of turbulent wakes from vortex streets.
Natl Advisory Committee Aeronaut., Rep.1191.
- [27] F. H. Shair and A. S. Grove and E. E. Petersen and A. Acrivos:
The effect of confining walls on the stability of the steady wake behind a circular cylinder.
J. Fluid Mech. 17, 1963, pp.546 – 550.
- [28] F. T. Smith:
Laminar flow of an incompressible fluid past a bluff body: the separation, reattachment, eddy properties and drag.
J. Fluid Mech. 1, 1979, pp.171 – 205.
- [29] J. S. Son, T. J. Hardy:
Numerical Solution for the flow around a cylinder at Reynolds number of 40, 200, 500.
J. Fluid. Mech. 35 (2), 1969, pp.369 – 386
- [30] M. Thompson, K. Hourigan, J. Sheridan:
Three-dimensional instabilities in the wake of a circular cylinder.
Experimental Thermal and Fluid Science 12, 1996, pp.190 – 196.
- [31] C. H. K. Williamson:
Defining a universal and continuous Strouhal-Reynolds number relationship for the laminar vortex shedding of a circular cylinder.
Phys. Fluids 31 (10), 1988, pp.2742 – 2744.
- [32] C. H. K. Williamson:
Oblique and parallel modes of vortex shedding in the wake of a circular cylinder at low Reynolds numbers.
J. Fluid Mech. 206, 1989, pp.579 – 627.
- [33] C. H. K. Williamson:
The natural and forced formation of spot-like vortex dislocations in the transition of a

- wake.*
J. Fluid Mech. 243, 1996, pp.477 – 539.
- [34] S. Wolfram:
Cellular Automaton Fluids 1: Basic Theory.
J. Stat. Phys. 3/4, 1986, pp.471 – 526.
- [35] D.A. Wolf-Gladrow:
Lattice-Gas Cellular Automata and Lattice Boltzmann Models.
Lecture Notes in Mathematics 1725, 2000
- [36] Y. Yokoi:
Vortex shedding from circular cylinder in a rectangular duct.
The National Defense Academy, Dept. of Mechanical Engineering Yokosuka, Japan
- [37] Th. Zeiser:
Numerische Simulation der instationären Umströmung eines quadratischen Zylinders mit einem Lattice-Boltzmann Verfahren.
Studienarbeit, Lehrstuhl für Strömungsmechanik, Universität Erlangen-Nürnberg, 1998
- [38] L. Zovatto, G. Pedrizetti:
Flow about a circular cylinder between parallel walls.
J. Fluid Mech. 440, 2001, pp.1 – 25